IRAM-283

Dynamics of molecular clouds in M51

S. Garcia-Burillo, F. Combes, M. Gerin

IRAM N°283

Astron. and Astrophys.
1993

DYNAMICS OF MOLECULAR CLOUDS IN M51

S.García-Burillo[1,2], *F.Combes*[3], *M.Gerin*[3]

Accepted for publication in Astronomy and Astrophysics

(1) *Institut de Radioastronomie Millimétrique, IRAM-Grenoble, 300, Rue de la Piscine, 38406 SAINT MARTIN D'HERES, FRANCE*
(2) *Centro Astronómico de Yebes, Apartado 148, E-19080 GUADALAJARA, SPAIN*
(3) *Ecole Normale Supérieure, Paris, and Observatoire de Meudon, 92190 Meudon, France*

A&A manuscript no.
(will be inserted by hand later)

Your thesaurus codes are:
07.02.1;07.07.1;07.09.1;07.14.1;09.09.1;18.05.1

ASTRONOMY
AND
ASTROPHYSICS

Dynamics of molecular clouds in M51

S.Garcia-Burillo[1,2] F.Combes[3] and M.Gerin[3]

[1] IRAM, 300 rue de la piscine, 38406 St Martin d'Hères, France

[2] Centro Astronómico de Yebes. IGN. 19080 Guadalajara, Spain Yebes Astron. Ctr,

[3] Ecole Normale Supérieure, Paris, and Observatoire de Meudon, 92190 Meudon, France
Radioastron. Meudon Observatory
Millimetrique

Abstract.

We analyse in detail the molecular gas dynamics in M51, by comparing the IRAM CO data obtained with 12" resolution (0.5 kpc) with the result of Monte-Carlo simulations of the cloud hydrodynamics, during the encounter with NGC 5195. Simulations are 3D and we do not consider gas self-gravity. The fit between the simulated result and the observed galaxy allows us to know the pattern speed of the spiral, and to locate the principal resonances in the disk, especially the corotation, the ILR and the OLR. We can then compare closely the arm-interarm contrasts and the kinematics of the molecular gas between the model and the observations.

We have succeeded in reproducing the high (3–5) arm-interarm contrasts observed in the ^{12}CO map simply by orbit crowding. The contrast is slightly higher in the simulation, but we find evidence of macroscopic opacity effects in the observations that could, by saturation, weaken the contrast. As expected from density wave theory, the arm-interarm contrast is everywhere higher in the near-infrared map than in the CO map. We find no evidence for a galactic shock either in the simulations, or in the observations.

The simulated and observed velocity fields are remarkably similar. In particular, the strong streaming motions observed both in the arm and in the interarm regions (60-75km/s in the plane of the galaxy with respect to purely circular motion) are reproduced by the model.

Send offprint requests to: S.Garcia-Burillo

The simulated and observed velocity-dispersion maps reveal maxima in the spiral arms. But the amount of velocity dispersion in the arms is higher in the observations. We discuss two possible explanations for the observed line-widths, accounting for such discrepancy.

First, we have studied the fueling of large-scale turbulence as a result of the dissipation of the kinetic energy provided by differential rotation in the disk, under the action of viscous torques. Although in the case of M51, it seems possible to account locally for the observed line-widths, the associated lifetime for the generated turbulence would be surprisingly short: after a $\sim$ rotation period the molecular gas disk would collapse towards the center.

An alternative explanation envisages the occurrence of "macroscopic" opacity effects; a substantial fraction of the CO emission comes from giant molecular cloud envelopes or "haloes", sub-thermally excited, at about Tex =5-7K. In the central spiral arms, the surface filling factor of these "haloes" is larger than one, even taking into account their velocity spread. This is supported by the low CO(2–1)/CO(1–0) ratio all over the galaxy, the narrower line-width in 13CO and the high surface filling factor observed in the simulations.

We find evidence for GMA (giant molecular associations) that are only an unbound random superposition of molecular clouds. Since the width of a typical spiral arm is a few times the diameter of a GMC, these GMA look like beads on a string.

Key words: Galaxies: barred; evolution of; general; kinematics and dynamics of; – Interstellar medium: clouds: general; – Radio lines: molecular

1. Introduction

Fig. 1. Adopted stellar surface density in the plane of M51: derived from a/Left: a red image (plate digitized by the MAMA), and b/Right: a near-infrared CCD picture from Gatley (private communication); we can see in 1.b/ the central part of the adopted surface density showing the stellar bar extending up to $R \sim 20''$

M51 is the prototype galaxy possessing a grand-design spiral pattern, and it offers the opportunity to check theories of density waves and of gas streaming motions through the pattern. In particular, the role of spiral density waves in triggering star formation is not

yet clear, and the distribution of molecular clouds across the spiral arms has received recently a lot of attention. While the spiral structure was barely resolved with the first single dish observations (Scoville & Young 1983; Rydbeck et al 1985), interferometric studies have progressively revealed the high contrast in the spiral distribution of molecular clouds (Lo et al 1987; Vogel et al 1988; Rand & Kulkarni 1990). The detected arms are very narrow and spatially coincident with the dust lanes, but they are offset from the ridge of Hα emission. A similar offset is seen between the dust lanes and the thermal radio emission (Tilanus & Allen 1988), which has been interpreted as a delay between the peak compression of molecular gas, and that of massive star formation.

Single dish observations with high resolution carried out at the IRAM 30m telescope (Garcia-Burillo & Guélin 1990, see also Garcia-Burillo et al, 1992 thereafter called Paper I) complete this partial view of the CO distribution, by revealing the large-scale emission for which interferometric observations are not sensitive. The observations are extensively described in paper I. We will briefly report here the main results of the observations (see below). Here we present hydrodynamic simulations of the M51 disk, to help interprete the results.

We compute the gas behaviour in a potential derived from infrared maps, perturbed by the tidal field of the companion galaxy NGC 5195. We then "observe" the simulated distribution, to predict the CO spectra all over the map. The fitting between the model and the observations allows us to understand the structure of the spiral, in particular to locate the principal resonances, and to check whether theory can account for the arm-interarm contrast and for the streaming motions. Finally, the model helps to disentangle in the observations what is due to the dynamics, and what to the local turbulence processes, or radiative transfer of the lines.

We first present here a short summary with the main results of the observations, especially those that constrain our model:

Molecular clouds in M51 are found to be distributed in a highly contrasted two spiral arm structure, with an average arm-interarm contrast between 3-5.5, having an increasing radial trend. Interarm emission is detected within the inner 5 kpc. The two spiral arms stretch out from a small inner molecular bar ending at R $\simeq$ 20". Kinematics of the gas is markedly affected by the density wave: strong non-circular motions of up to 75 km/s (measured both in the interarm and in the arm region, with respect to circular rotation) in the plane of the galaxy are detected. No change of sign for the radial streaming motions along the kinematical minor axis (predicted by density wave theory) is visible up to a distance of 6.7 kpc. That gives a lower limit for the location of corotation in the disk.

Noncircular motions are also present in the inner region associated with the bar. These clearly suggest that molecular clouds are trapped in elliptical orbits whose major axis (as viewed from the *wave* rotating frame at Ω_p) is close to the stellar bar one. Second order moments maps indicate that velocity dispersion is higher in the arms, compared to the interarm region. Line-widths can locally reach values as high as 60 km/s. Another observational result which seems relevant for the validity of the hypothesis assumed in the model, is that molecular gas largely dominates the neutral gas content of the disk. HI is very defficient in the inner disk. Only at large radii (out of the simulations scenario) neutral hydrogen abundance is of the same order of magnitude than molecular gas.

We describe in section 2. the numerical method used in the simulations, the derivation of the gravitational potential, and the details of the tidal interaction parameters. The results are presented in 3., where we compare the predicted map to the observations. Finally, we discuss the implications for the interpretation of the CO observations in section 4.

2. Methods

Our simulation is based on gas streaming in a potential as close to the real one as possible, with no self-gravitation.

2.1. Determination of the potential

We combine a red plate image, digitized with the automatic machine called MAMA in the Paris observatory, with a near-infrared CCD picture at 2.2 μ, provided by Gatley (1990, private communication). The maps are complementary. The NIR picture does not have enough signal to noise ratio in the disk regions, and the spiral structure is not as beautifully defined as in the red photograph. The red plate suffers from saturation problems in the center (inside a radius of 20", or about 1 kpc), where the NIR picture indicates a high increase of surface density, and where it is possible to distinguish a small stellar bar (Fig. 1). An oval distortion has also been reported by Pierce (1986) and Zaritsky & Lo (1986). The position angle of this distortion is 135°, and the maximal axis ratio 1.5; its extent is 20". The end of the bar corresponds exactly to the beginning of the inner spiral arms, that form a ring-like structure in the CO data.

For the inner disk of 20" radius, we adopt for our model of the stellar surface density the NIR picture, and the MAMA red image outside. At the radius of 20", the two pictures were joined up to the same intensity. In this way, we account for the different M/L in the two bands. Once the stellar surface density is derived in this manner (in arbitrary

units), we deproject it to obtain the corresponding quantity in the galaxy plane ($i = 20°$, $PA = 170°$). The potential is then computed by a Fourier transform on 256 x 256 pixels of 1.76" x 1.76" size, assuming a constant M/L ratio over the disk in the first iteration. The comparison of the derived rotation curve with the observed one requires to modify the mass-to-luminosity ratio as a function of radius. We were led to increase M/L more in the region 0.5<R< 3 kpc, certainly because of the large absorption from dust. The M/L ratio reaches at 1kpc a peak of twice its central value, and decreases smoothly afterwards. Indeed, from the CO emission, this region corresponds to a pseudo-ring where we derive extinctions of $A_v = 5 - 7$ mag, averaged over the beam of 540 pc in size. We also add a small spherical bulge (a Plummer component of radius 3kpc) of mass $1 \times 10^{10} M_\odot$, i.e. 0.01 of the total mass, corresponding to the late type (Sc) of M51. Although the rotation is almost flat in the simulated region, it was not necessary to add any massive halo.

The potential is extended perpendicular to the plane, by the assumption of cylindrical symmetry (i.e. x and y forces independent of z), since we are concerned only with the molecular gas of thickness 50 pc. In the inner parts (inside 7 kpc radius), there is no observational evidence of plane warping, even in HI (Rots et al 1990); *a posteriori*, the model does not show either any evidence for large gas excursion in z. For the z forces, we assume that the stellar plane obeys the equilibrium of an infinite layer, with a density $\rho = \rho_o \times \mathrm{sech}^2(z/H)$, where H is the scale-height; we adopt H=1 kpc.

2.2. Numerical method

The hydrodynamics of the gas is simulated with the collisional model described in Combes & Gerin (1985), extended in three dimensions. Clouds are distributed according to a mass spectrum from 10^3 to $10^6 M_\odot$. They interact via collisions, that can result in coalescence, mass exchange or fragmentation. Their number is therefore not constant, but can reach a maximum of 4×10^4, and is on average 2×10^4, the total mass of H_2 being conserved in the simulation. To determine the collisions, we superpose a grid to the ensemble of particles, whose cell size is proportional to the mean free path corresponding to the mass of the cloud. Although we follow clouds orbits in 3D, the collision grid is kept two-dimensional, and is at maximum 240 by 240. Indeed the spatial resolution to determine these collisions is at most 85 pc, which is of the order of the thickness of the plane of molecular clouds. During the tidal interaction, particles can move freely in the z-direction, but the deformation of the plane was never so large that a third dimension in the collisional grid was necessary, even though the orbit of the companion is not in the M51 plane.

The spatial resolution of the simulations is determined both from the collision cell (85pc) and the gravitational cell (80pc), since any gradient on smaller scales will be smoothed out in the forces calculations. This spatial resolution is appropriate to compare the gas behaviour with the IRAM observations, with a beam of 550pc. However, we might slightly underestimate the streaming motions gradients (see section 3.4.2).

Fig. 2. Adopted rotation curve in the plane of M51, derived from the stellar image of figure 1, with the M/L described in 2.1, so as to fit the CO rotation curve from paper I.

Clouds over $3x10^5$ $M_\odot$ are called GMCs (giant molecular clouds): they can be dispersed by star formation after a life-time of 4x 10^7years (e.g. Bash 1979). When a GMC is dispersed, its mass is re-injected to the interstellar medium in the form of small clouds, with a velocity dispersion of 10km/s. This accounts for the energy provided locally by star formation, and is necessary to compensate for the energy dissipated in collisions, which would have implied the viscous collapse of the gas towards the center. In the absence of any perturbation, in an axisymmetric potential, the molecular clouds are in a quasi-equilibrium, distributed with the mass spectrum that ensures balance between dissipation and energy re-injection. We have varied the collision parameters (cross-sections and velocity dispersion after GMC dispersion). These factors, especially the first, have not been found to be much critical. In fact, a quasi-steady equilibrium is reached in the clouds ensemble, the dissipation by collisions being compensated by the energy reinjected at GMC dispersion. Only when the velocity dispersion reaches 25km/s, the gaseous spiral arms are significantly wider and the spiral structure tends to appear washed out. We therefore kept a value of 10 km/s for the energy reinjection after GMC dispersion.

Clouds are considered as test particles in the potential determined in 2.1. More precisely, the potential is decomposed in its axisymmetric and non-axisymmetric parts. Initially, the particles are launched with the rotational velocity in the axisymmetric potential, with a small velocity dispersion in the plane (10km/s). The non-axisymmetric perturbation is then introduced gradually, with a time-scale corresponding to the time elapsed since pericenter, a fraction of the orbital period of the companion: we consider that the spiral density wave is entirely due to the tidal interaction. The perturbation is given a constant angular velocity Ω_p, a free parameter that we have varied to obtain a good morphological fit with the observations.

The initial radial distribution of molecular clouds is an exponential disk of scale ad = 2.4 kpc. Its distribution perpendicular to the plane is gaussian, as expected from the

Fig. 3. Particle plots representing gas clouds in the M51 disk, for several runs: a) Ω_p = 40km/s/kpc; b) Ω_p = 20km/s/kpc; c) Ω_p = 10km/s/kpc; d) Ω_p = 27km/s/kpc, the best fit.

equilibrium of a multi-component system (Talbot & Arnett 1975). Its thickness is hd = 50pc, and its velocity dispersion in z is $\sigma_z = \mathrm{hd} \times (2\pi G \rho_o)^{1/2}$, with ρ_o being the total (mainly stellar) density in the plane. This density is computed from the red image and the M/L ratio fitted to the rotation curve (see section 2.1).

2.3. Tidal interaction

The companion is schematised by a Plummer potential, corresponding to a mass ratio of about 1/4 with M51: $\Psi = GM_c(r^2 + a_c{}^2)^{-1/2}$, with M_c and a_c being the mass and the characteristic size of the companion, respectively $2.3 \times 10^{10} \mathrm{M}_\odot$ and 1.6 kpc.

Its orbit has been calculated around the potential of M51 composed of a thin disk and bulge, in two steps. A first guess of the orbit was obtained by fitting with a 3-body code an ellipse of excentricity $e = 0.8$, and inclination $i = -70°$; the pericenter angle is $\omega = -15°$ and the viewing longitude is $\lambda = 65°$, parameters very close to that from Toomre & Toomre (1972). The pericenter distance is 13 kpc, reached 8×10^7yrs before the present time. Then, to make the orbit correspond more closely to the potential chosen for M51, we integrate back in time from the present, with the obtained relative 3D position and velocity, in the exact potential. The orbit is no longer an ellipse, but is still approximate, non including dynamical friction. It accounts for the external tidal perturbations, assumed to be material arms. The orbit is bound, which must correspond to the reality: it is indeed suspected that the companion NGC 5195 has turned around M51 for at least two revolutions, from the recent VLA HI observations (Rots et al 1990), that show an extremely extended tail in the outer parts.

Fig. 4. Particle plots for runs where Ω_p= 27km/s/kpc, but where the shape of the rotation curve is varied in the center: a) no ILR exists; b) there are 2 ILRs.

3. Results

3.1. Model fitting

We ran several models, varying the pattern angular velocity Ω_p. The gas response is very sensitive to this parameter: we obtain a spiral structure similar to what is observed for

only a narrow range of Ω_p. Fig. 3 shows the final morphologies obtained for some of these runs. The gaseous spiral arms are not in phase with the stellar arms of the underlying potential, when Ω_p is far from 27km/s/kpc. This value is very close to the maximum of the $\Omega - \kappa/2$ curve, and somewhat higher than the angular velocity of the companion at pericenter (22km/s/kpc).

For Ω_p = 40km/s/kpc, the outer gaseous disk reveals only weak structures; this is easy to understand since in a two-armed pattern, the periodic orbits that support the structure are elongated like ellipses, and their major axis precess around the center at the rate $\Omega - \kappa/2$. If the imposed pattern speed rotates at a much higher rate, the particles just see an axisymmetric potential in average, and not a spiral one. The particles however are subject to the companion tidal forces, but those are particularly strong at larger radii, where the density of the molecular component drops.

For Ω_p = 20km/s/kpc, a contrasted spiral structure develops in the molecular gas, but it soon precesses at a higher rate than the imposed stellar spiral arms, which trails behind. In the center, the gas settles in a barred structure perpendicular to the observed stellar bar. This might correspond to the periodic orbits expected perpendicular to the bar between its two inner Lindblad resonances, when they are present (Contopoulos & Papayanopoulos 1980). Such a perpendicular gas bar is not seen either in the morphology nor the kinematics of the molecular gas. The perpendicular structure disappears for Ω_p = 10km/s/kpc (fig. 3).

Fig. 5. Particle plots of the best-fit run. Clouds are displayed according to their real sizes, and it is clear that there is considerable overlap, mainly in the arms. The cloud ensemble plotted here corresponds to $10^9 M_\odot$, while 10 times more mass is observed in M51.

To obtain the best fit, we proceeded in two steps: variation of Ω_p with a fixed rotation curve to get the outer spiral, then variation of the mass distribution in the center (modification of the M/L ratio). Indeed, the rotation curve is not well known in the center. There exist strong non-circular motions due to the central bar, and the kinematical data in this region overestimate the axisymmetric rotation velocity. Fig. 4 shows the effect of varying the central mass distribution. Essentially, when the maximum of the $\Omega - \kappa/2$ curve is high enough, we obtain a strong gas bar along the stellar one, since more gas can be trapped in resonant orbits. When it is too low, the gas response can rotate by any angle with respect to the stellar bar.

For the best-fit model, Ω_p = 27km/s/kpc, we find just one ILR at 1.7 kpc, the corotation at 7.4 kpc and the OLR at 11.1 kpc. The ILR corresponds exactly to the position of the pseudo-ring in the CO distribution, at the end of the oval distortion seen in the infra-red maps. The corotation corresponds to the the outer optical arms.

The action of the companion is accounted for in these simulations through two effects: first the direct tidal forces, second the presence of the density wave in the adopted potential. Since we are concerned with the inner disk, the second action is expected to dominate. Indeed the direct tidal forces roughly vary as the square of the radius in the M51 plane. We tested the influence of direct tidal forces by running a simulation without companion, and it appears to be very similar to the best-fit simulation, where the companion was included. Therefore, the choice of the companion orbit is not critical.

3.2. Observation of the model

To better compare with the observations, we "observe" the result of the simulations, i.e. we compute the projected quantities (positions and radial velocities of each cloud), and produce a data cube by convolution of the expected emission of all clouds by the telescope beam. The cell size of the cube is half the resolution, i.e. 6" in the spatial dimensions of the cube, and 3km/s in velocity.

We assume the clouds to be homogeneous and spherical. Their integrated emission is proportional to their mass. Although molecular clouds are optically thick in the CO line, it is believed that there is a proportionality factor between integrated intensity and total H_2 mass (Bloemen et al 1986). Each cloud emits a gaussian CO spectrum, with an intrinsic velocity dispersion related to its mass, according to the relations observed in our own Galaxy (e.g. Solomon et al 1987): the velocity dispersion $\sigma_v \propto size^{0.5}$, and the $size \propto M^{0.5}$. We adopt the relation $\sigma_v(km/s) = 0.23M(\mathrm{M}_\odot)^{0.25}$ which makes the velocity dispersion vary from 1.3 to 7.4km/s for clouds between 10^3 to 10^6 $\mathrm{M}_\odot$ (i.e. line-width at half-power between 3 and 17km/s).

Note that the above relations imply that the average column density $N(H_2)$ is constant for all types of clouds, provided that they are resolved (the average CO emission is also constant). But here the clouds are not resolved by the beam (12" = 550 pc), which is the case for most extragalactic studies. Then each cloud contribute to the total emission according to its dilution factor, proportional to the square of its size, i.e. to its mass.

When summing CO emissions in each pixel, we are confronted to the problem of optical thickness of the ensemble of clouds. There is no doubt that individual molecular clouds are optically thick in the CO line, as testified by the observed ^{13}CO isotopic ratios (Paper I).

However, it is generally assumed that clouds are macroscopically optically thin, i.e. that clouds do not hide each other at some given radial velocity. This assumption is at the basis of the widely used standard H_2/CO conversion ratio: the CO emission is proportional to the H_2 column density, since we are counting the number of "standard" clouds in the beam. But in the model (see fig. 5), it is clear that clouds are overlapping towards some line of sights. Yet we have simulated (and plotted in fig. 5) only one tenth of the real number of clouds. We have indeed $10^9 M_\odot$ in the model, compared to $10^{10} M_\odot$ observed in M51. We therefore "observe" the simulations in two alternative ways: 1) assuming that the CO emission of clouds is macroscopically optically thin (CO emission proportional to the cloud mass); 2) taking into account cloud overlapping at a given velocity. In the latter choice, for each pixel we sort out clouds according to their position along the line-of-sight. The first cloud contributes a CO emission proportional to its mass, and spread around its radial velocity, according to its intrinsic dispersion. Then the successive clouds are projected against all clouds before them. We compute the overlapping area in function of their relative positions and sizes; and in each common velocity channel, we absorb the CO emission with a thickness proportional to the column density of all foreground clouds at this precise channel. We do not treat the radiative transfer problem of course, but we take into account the main effect of cloud overlapping at each velocity. This procedure saturates the emission in the central regions and in the arms, and widens the spectra, which then correspond better to the observations (see below).

3.3. Comparison between the modelled and the observed intensity maps

3.3.1. Arm position, pitch-angle

Fig. 6. Superposition of CO intensity maps: the grey-scale represents the model, the contours are from the observed distribution.

Fig. 6 displays the superposition of the observed and modelled intensity maps. The arms coincide in position, in particular the inner arms. The pitch angles are therefore comparable in the model and in the observations. The outer arms appear thinner in the model, but are less well determined in the CO observations. The arms are punctuated by big clumps, that have been called giant molecular associations (GMA) by Vogel et al (1988) and Rand & Kulkarni 1990. Such clumps are also visible in the simulated map, where these associations are not bound, since we do not consider self-gravity in our simulations. We can wonder whether these structures can easily be obtained by random superposition

Fig. 7. "Observation" of the same ensemble of clouds as in fig. 5, but now randomly distributed: a) in all the frame; b) only in strips of 1 kpc wide.

of molecular clouds and GMCs. To answer that, we have re-distributed in position the whole ensemble of clouds considered in the simulation of fig. 5, with their own masses. When the clouds are randomly distributed within the same area, we obtain what is displayed in fig. 7a, with a maximum intensity contrast of 10 between all pixels. When the same clouds are randomly distributed in strips of 1 kpc wide (fig. 7b), we then obtain structures very similar to the observed ones. This can be understood since stochastically, associations of GMCs are expected with an average size of 500pc-1kpc, the width of a spiral arm. Only one such cluster can occur across an arm, and they are forced to look like beads on a string.

Rand & Kulkarni (1990) have investigated the same question, and came to the opposite conclusion: GMAs cannot be random associations of clouds, but must have a dynamical origin. This may come from two facts: in their simulations, they have not tried to distribute clouds in spiral arms, which we believe is the essential geometric ingredient (mainly the ratio between the width of an arm and the GMC diameter); and they have tried to fit the GMA's contrast seen in interferometric work, which is overestimated with respect to that obtained with single dishes. Lo et al (1991) have beautifully shown that 70% of the CO emission missing in the interferometric maps has to be added in the spiral arms. Arms appear wider, as noted by Garcia-Burillo and Guélin 1990, and the contrast of their sub-concentrations is smaller.

What is obvious in the model and also in the observations, is that the arms have an almost symmetrical profile in azimuth (fig. 8). There is no significative sharpening at the entrance of the arms neither in the model nor in the observations, as it could be expected if the gas experienced a shock. Here, we consider ballistic clouds in collisions, and an equivalent "shock" could only occur along a mean free path, of the order of 200 pc. That explains why there is no galactic shock apparent here.

Fig. 8. Azimutal profiles across spiral arms; a) observations, b) model(optically thin), c) infrared picture., for three rings of 0.5 kpc width, at $R = 3.2$ kpc and $R = 5.4$ kpc, deprojected in the plane of the galaxy. The intensity scales are arbitrary. The azimuth units are degrees

3.3.2. Arm-interarm contrasts

In our simulations, arm-interarm contrasts are the result of orbit crowding along the spiral arms. The effect of formation of molecular clouds from diffuse neutral gas complexes by gravitational instability is not included (even if it is implicitely accepted). We assume that the giant clouds, after their dispersion by star formation events are immediately recycled in the molecular phase, at the small mass end of the spectrum.

M51 has a high molecular gas content: nearly 90% of the neutral gas is molecular. The density wave present in the disk might just concentrate pre-existing molecular clouds along the spiral arms (its role in the formation of H_2 from HI complexes being secondary, at least at the "present time"). Our simulations can test the validity of such hypothesis in M51, where accurate arm-interarm contrast have been measured for CO.

When we compare the model and the observations, arm-interarm contrasts (defined as $<I_{arm}>/<I_{interarm}>$ at the same galactocentric distance) agree satisfactorily within the errors. Such agreement is even better, once we take into account the effect of "macroscopic" opacity (section 3.2). In fact, from the "optically thin" simulated cube we obtain slightly higher arm-interarm contrasts (see Fig. 8). Consequently, our simulations suggest that the arm-interarm molecular mass ratio might be higher than the corresponding CO integrated intensity ratio. In that case, molecular gas column densities could be slightly underestimated (see below).

In the model, as well as in the observations, arm-interarm contrast increases with galactocentric distance up to corotation. Such a radial trend for the contrast is not surprising: in the inner disk, complex of clouds do not have enough time to disgregate completely between each passage of the density wave. This situation changes at increasingly larger radii. Moreover, arm-interarm contrasts are underestimated within the inner 30" by lack of spatial resolution.

Arm-interarm contrast for the stellar surface density, derived from the infrared and red images, are systematically a factor of two smaller than the CO ratios (which is not surprising in density wave theory standards)

3.3.3. Central ring

The main feature of the intensity map (in the model and in the observations) is the presence of a ring-like structure in the center, that corresponds to the beginning of the two spiral arms. The highest surface density of molecular gas is found in the ring, both in the model and in the observations (see fig. 11). The initial radial distribution of

the model was exponential, with a scale-length of 2.4 kpc, the formation of the ring is therefore a purely dynamical phenomenon, due to gravitational torques, as described in Combes (1991). The mean radius of the ring corresponds to the inner Lindblad resonance. The overall orientation of the ring is however not elongated along the bar, but more in the perpendicular direction. This is also confirmed by the kinematics (see below).

3.4. Comparison between the modelled and the observed kinematics

3.4.1. Departures from circular motion

The iso-velocity curves of figs. 9 and 10 reveal strong streaming motions, both in the model and observations, and with the same order of magnitude. In the major-axis cut (fig. 12), we see that the gas is rotating more rapidly at the outside of the arms, which is expected from the density-wave theory. Also, along the minor-axis cut, (fig. 13) the gas is rotating faster outside the arms, which is expected inside corotation. There is so few CO emission outside what we find to be the corotation radius, that we cannot check the reversal of these radial streaming-motions, as expected from the theory . Surprisingly, in the HI map (Rots et al 1990) there does not seem to be such a reversal, even if the HI disk extends outside the location of corotation as derived in our model: when crossing the outer spiral arm on both sides along the minor axis, gas still moves inwards (as inside corotation). Moreover, the outer arms could belong to a different pattern and they might be inside a *second corotation.*

Fig. 9. Isovelocity curves from the observed CO distribution. Contours are from 410 to 520 by 10km/s.

Fig. 10. Isovelocity curves from the model. Contours are the same as in fig. 9.

Fig. 11. Average normalized radial distributions of molecular gas in the observations (dashed line) and in the simulations (solid thick line).

In the very center (inside 20"), the isovelocity contours are not perpendicular to the major-axis ($PA = 170°$), but are rotated by 10° or so ($PA = 180°$). This occurs both in the model and in the observed map (fig. 9). This is the symptom of non-circular motions due to the oval distortion. There are some gas clouds in the very center, in orbits parallel

to the optical bar. Perpendicular orbits would have made the isovelocity contours rotate in the other direction. However, as shown by the velocity field in the rotating frame of fig. 14, these orbits parallel to the bar do not extend farther than a radius of 1 kpc (or 20"). As soon as the end of the optical distortion, the gas settles in orbits elongated in the perpendicular direction, to form the ring. The major-axis of the orbits then turn gradually to form the spiral arms. These non-circular motions are traced by undulations of the isovelocities at the position of the ring.

Both the intensity map (maxima in two opposite regions NE and SW, on both sides of the nucleus) and the kinematics constrain the orbits of the gas in the ring to be perpendicular to the bar.

3.4.2. Velocity dispersion

In the model, as well as in the observations, the velocity dispersion is particularly high in the center on the minor axis, and in the arms (fig. 15). In the optically thin model, this situation is expected since there is a large velocity gradient on the minor axis, due to projection effects, and in the arms the streaming motions widen the spectra: they are not entirely resolved out. To test this hypothesis we have analysed the Hα map of Tully (1974). This higher resolution Hα map reveals twice higher amplitude for the streaming motions (Tully 1974). Interarm diffuse Hα emission seems scarce at some locations and the gas kinematics there is poorly determined. Nevertheless, whenever Hα is clearly detected both in the arm and in the interarm region, we can estimate that streaming motions are always twice higher compared to what we see in CO. That is undoubtedly a resolution effect. These very high streaming motions are confirmed by a recent Hα Fabry-Perot study from Vogel et al (1992): 150km/s departures from a circular velocity field are observed in the plane of the galaxy (instead of 60-70 km/s measured in CO)

Fig. 12. North-South position-velocity cut for the observations (top) and model (bottom). This is almost the major-axis cut.

Fig. 13. East-West position-velocity cut for the observations(top) and the model(bottom). This is almost the minor axis cut.

Also, in the center, the non-circular motions due to the oval distortion, and the higher z-velocities are factors that can explain the increase of line-widths.

Fig. 14. Velocity field in the rotating frame of the model, displaying gas orbits.

The velocity dispersion in the z-direction, may not be well represented in the model. We know neither the shape of the stellar potential perpendicular to the plane, nor the thickness of the gas plane. The z-velocity dispersion of the gas (σ_z) is proportional to the thickness hd, that we have assumed to be 50 pc, and to the square root of the volumic stellar density, which we do not know; we have assumed the stellar thickness around 1 kpc and the bulge/disk ratio to be very small. We estimate the uncertainty in σ_z to at least a factor 2. For the parameters adopted in the model, z-velocities barely widened the spectra, but it could have a significant effect for thicker gas planes. The tidal interaction do not significantly alter the z-equilibrium of the gas plane, although the companion orbit is far from coplanar to M51. This is because we are concerned here with the inner parts, where the tides are relatively weak.

Fig. 15. Contours of velocity dispersion superposed on the intensity map (grey-scale) for a) observations; b) model. Contours are from 10% to 100% by a step of 10% of the maximum value.

There is an important discrepancy between the optically-thin model and the observations: throughout the spiral arms, the CO line-widths are twice wider in the observed spectra (40km/s in average with respect to about 20-30 km/s in the model). On the contrary, the widths are similar in the interarm regions (about 10-20km/s). There is also a region of the southern arm (centered at 30",-54") where the observed spectra are much wider, 60km/s (FWHM), than the modelled spectra, which are never larger than 30km/s, at half-power.

A detailed comparison shows that the observed spectra are not only wider, but at some places they are asymmetrical: the model spectrum always falls on one side only of the corresponding observed one. The widening cannot therefore be due to a larger z-velocity in the observations, since we would then expect emission symmetrically on both sides of the model spectra. Since the asymmetry follows the rotation structure of the galaxy, the widening must be in the plane (see Fig. 16). What is the source of the widening?

Streaming motions could indeed widen in part the spectra, since we know from Hα observations that the gradient is stronger than that detected in the CO map. However,

the simulations, with a spatial resolution of 80pc, take them into account more exactly and yet the derived spectra are not enough broadened. We believe that the streaming motions in the model are of the right order of magnitude, since they are reproduced with about the same intensity (15–20km/s in radial projection) as in the CO map, at the same resolution.

The same is true for systematic gradients due to the rotation: we have plotted in fig 17a the average line-width in function of radius when these systematic motions are taken into account or not (we substract the expected line-width at each location). It is clear that the line-width is not dominated by the rotational gradient.

The only two interpretations of these large line-widths throughout the spiral arms are large-scale turbulence, and opacity. The former hypothesis requires huge amount of turbulence, whose origin is not known. This cannot be generated by star-formation activity (supernovae, stellar-winds, HII regions), since this has been estimated to 10 km/s at most. The only reservoir of kinetic energy could be the rotation of the galaxy itself, and the shear due to differential rotation could dissipate this energy by viscous torques (Fleck 1981). But the dissipation time with such a huge turbulence is very short, of the order of a rotation period. That means that the gaseous disk should collapse towards the center in 2×10^8 yrs. This is difficult to understand, especially since the companion must have made at least two passages around M51.

The alternative interpretation, an opacity effect of the CO lines, looks more reasonable, since we already noticed that the clouds were overlapping. We discuss in more details the consequence of this hypothesis in the next section.

Concerning the region in the southern spiral arm where ^{12}CO line-widths are exceptionally large, it has been shown in paper I that the ^{13}CO line is double-peaked, while the ^{12}CO spectrum has a wide flat-topped shape. This suggests either an unresolved exceptionnally large streaming gradient (as it is suggested by a close inspection of the Hα velocity map, Tully (1974), Vogel et al 1992), or the existence of a large expanding shell in this arm region.

4. Discussion

4.1. Model hypotheses

4.1.1. A single pattern

The main constraining hypothesis in our model is that the spiral structure of M51 is represented by a single pattern, with a given constant angular velocity Ω_p. It is however

likely that in case of spiral waves excited from outside, as is the case in a tidal interaction, two patterns develop: one with an angular velocity characteristic of the potential of the galaxy in the inner parts, and one corotating with the companion in the outer parts (Combes 1991). The first pattern extends at least until its own corotation, which in the case of our simulation encompasses most of the molecular gas. Indeed, no reversal is seen in the radial streaming motions along the minor axis within the inner 160", from the observations (paper I). Therefore, we believe that our gas particles are indeed submitted to one single pattern and that our simulation scenario is located inside corotation.

4.1.2. A single passage

Fig. 16. Comparison of CO spectra from the observations and model, when the emission is assumed optically thin at the offset (RA,DC)=(0,-48)

Fig. 17. Left:Fig 17a: Radial distribution (azimuthally averaged) of line-widths (FWHM) in the observed distribution; full-line, direct measurement; dashed-line, when rotation velocity gradients are subtracted in each beam. **Right**:Fig 17b: Comparison of line-widths derived from the observations [III], the "optically thin" simulated cube [II] and the "optically thick" simulated cube [I]; in this picture, the rotational gradients have not been subtracted

The simulation begins when the companion is at its apocenter (about 22 kpc), and we do not take into account the previous passages. This approximation of course is too rough for the outer parts of the galaxy, where the HI tail will not be accounted for. But in the central parts, where is confined all the CO emission and presumably the molecular hydrogen, the tidal interaction has essentially indirect action: the inner spiral comes from the swing amplification of a small perturbation excited in the outer parts. The waves will develop in a rather short time, proportional to the dynamical time in the center, but they will fade away in a similar time-scale (Hernquist 1990, Howard & Byrd 1990). One can then expect that such spiral waves will be generated at each pericenter of the companion, and forget about the previous passages. Direct tidal forces were shown to be not critical for the molecular component in section 3.1.

4.1.3. Time-scale of the perturbation setting

The amplification time for the spiral waves to develop depends essentially on the rotation period of the matter concerned (Toomre, 1981). Particles located at 3 kpc from the center (in the middle of the CO disk) have a period of 8×10^7yrs, corresponding to the time elapsed from the pericenter, the characteristic time-scale chosen to set the spiral perturbation. Therefore, the time-scales are synchronized on average, but of course, the amplification time might be shorter in the center, and longer in the outer molecular disk. We have therefore introduced the non-axisymmetrical part of the potential on a time-scale of 8×10^7yrs.

Fig. 18. Left: Average ratio between I(CO) and ΔV in function of radius for the observed distribution. **Right**: Observed azimuthally averaged integrated intensity I(CO) in function of radius.

4.2. Line-widths

The large discrepancy between the width of the spectra in the observations and in the optically thin model, led us to consider cloud overlapping, i.e. macroscopic thickness (see section 3.4.2). This phenomenon must be distinguished from what we will call "microscopic thickness" in comparison, i.e. individual clouds are optically thick in the CO line; we consider them here similar to the ensemble of clouds in our own Galaxy.

To investigate further this hypothesis, let us estimate the surface filling factor of giant clouds or molecular complexes in one typical 12" beam. It can be expressed by $f = N \times \pi r^2/(beam - area)$, where N is the number of GMCs of $10^6 M_\odot$, with a radius r = 100 pc. A lower limit of N is obtained from the integrated emission I(CO). Since in the central spiral arms, I(CO) can be as high as 30Kkm/s, the column density $N(H_2)$ is of the order of $10^{22} mol \times cm^{-2}$, assuming the standard conversion ratio of 3 $10^{20} mol \times cm^{-2}$, derived for the Milky Way clouds. The mass contained in one beam is therefore of the order of 4 $10^7 M_\odot$, and $N \geq 40$. We then find a surface filling factor of $f \geq 5.2$. Of course, we have now to take into account the spread in velocity, and to compute a surface filling factor in each channel; if we take an intrinsic width at half power of 17km/s for GMCs (7km/s in dispersion), the filling factor f_v is ≥ 2.2 for the typical line-width seen in a spiral arm, 40km/s. This final filling factor larger than 1 strongly suggests that clouds are overlapping in the beam, and hiding each other.

If we try now to estimate this filling factor f_v all over the map, we have in fact to consider a quantity proportional to I(CO)/ΔV, where ΔV is the line-width, i.e. a quantity proportional to the peak antenna temperature. This quantity is plotted in fig. 18 in function of radius, and is indeed quite flat all over the map as opposed to the peaked integrated intensity distribution. By comparison, in the optically-thin model, the variation of this quantity is a factor 10 more. The radiation temperature is of the order of 1K, which can be interpreted as the average brightness temperature of the molecular emission. This can be interpreted as highly diluted emission from molecular cloud cores together with the emission of sub-thermally excited envelopes of GMCs. In our own Galaxy, large-scale surveys have revealed the existence of such emission (Polk et al 1988), with peak CO temperatures lower than 2K, and high ^{12}CO/^{13}CO intensity ratio (up to 6.7).

Fig. 19. Comparison between ^{12}CO and ^{13}CO observed spectra. at the offsets (RA,DC)=(0,18). The line-width are narrower in the less optically thick line.

Another element supporting the opacity hypothesis is the evolution of the line-width in HI, from what is known for other galaxies. For face-on galaxies of the same type, it has been shown that the velocity dispersion of the atomic gas varies only little with radius (van der Kruit & Shostak 1982, 1984; Shostak & van der Kruit 1984; Dickey et al 1990). It increases slightly towards the center, but is never larger than 15km/s. An increase towards the center is expected if the stellar density increases there, while the gas thickness remains the same. The HI width gives the order of magnitude of the expected CO width in the absence of opacity effects. Since the HI plane thickness is of the order of three times larger than that of the molecular gas in edge-on galaxies, the 1D CO line-width should be at least 3 times lower. We therefore expect a FWHM of 12km/s in CO.

Table 1. We can see the comparison between the observed line-widths estimated from the ^{12}CO and ^{13}CO line profiles at some positions, in the disk of M51. ^{13}CO line-widths seem systematically smaller than the ^{12}CO values.

Finally, we show in fig. 19 the comparison between one ^{12}CO and ^{13}CO spectrum observed towards M51. It can be seen that the ^{13}CO line-widths are smaller; this cannot be due to the structure of individual clouds, since the width is dominated by cloud-

cloud velocity dispersion, but this can be explained by a smaller "macroscopic" optical thickness in ^{13}CO, provided that the spectra are widened by opacity (see also Table 1). This effect has been reproduced in the simulations: reducing the adopted optical thickness significantly reduces the line-widths. It seems however that the ^{13}CO line is not always optically thin either.

Table 2. We compare the CO line-widths (FWHM) observed in the disks of some spiral galaxies

The blending of clouds in the beam helps to increase the line-width of the spectra in the arms, from 20-30 kms^{-1} to 40 kms^{-1} in FWHM (see Fig. 17b). Consequently, CO emission could be no longer a good tracer of molecular gas mass, at least in the arms.

The alternative factor of broadening the line-widths is large-scale turbulence. Such a large turbulence (up to 60km/s) is not usual in the molecular component. The internal dispersion of the Milky Way's GMCs, attributed to turbulence contributes at most 18km/s to the linewidths (Solomon et al 1987). This local turbulence is in general attributed to processes related to star-formation activity: expanding HII regions, supernova explosions, stellar winds, hydromagnetic waves (McKee & Ostriker 1977; Myers & Goodman 1988). Another manifestation of turbulence is through the high velocity wings recently investigated by Falgarone & Phillips (1990). They show that many molecular profiles can be decomposed in two gaussians, the width of the pedestal being 3.3 times the width of the main component. The existence of this pedestal is attributed to intermittency, a fundamental property of turbulence (Falgarone & Phillips 1990), or to hydromagnetic waves (Elmegreen 1991). These wings are however detected only with good signal-to-noise in our Galaxy, and would not be seen in external galaxies. We have tried to include this phenomenon in the "observation" of the simulation, and it did not produce enough line-broadening to explain the widths in M51.

These generate only small-scale turbulence, under 100 pc. Larger-scale turbulence can only be fueled by the differential rotation of the galaxy. The dissipation of the rotational kinetic energy in a galactic disk can be driven by viscous torques, a phenomenon investigated for accretion disks by Lynden-Bell & Pringle (1974). The amount of viscosity is crucial to determine the efficiency of the phenomenon. The viscosity must come from turbulent motions of the interstellar medium. Small-scale turbulence gives characteristic times of the dissipation of rotational energy (and collapse of the gaseous disk towards

the center) of the order of the Hubble time. In our Galaxy, the characteristic length of the generated turbulence is l=200 pc, and the associated characteristic motion v_l = 10km/s (Fleck 1981). We have calculated the magnitude of the turbulence predicted by this model in the disk of M51. Assuming the same z-scale height for the molecular gas in M51 and in our Galaxy (and that is a crucial assumption), we can estimate v_l from the value derived for A, the Oort constant (defined as $A = 1/2(\Omega - d(\Omega r)/dr)$), by

$$v_l/l \sim 2A \tag{1}$$

We find a value of v_l that stabilizes at 20 kms^{-1} for most of the disk, reaching a local maximum of 50 kms^{-1} at 2 kpc. The maximum velocity dispersion measured is $25kms^{-1}$, and since it is a 1D measurement, we derive an observed 3D $\sigma = 43kms^{-1}$. So it may be possible to generate locally, large scale turbulence from the differential rotation in the disk.

Another mechanism to generate turbulence, and turbulent viscosity, is the gravitational instabilities themselves (Lin & Pringle 1987): if the gas is too cold, i.e. its velocity dispersion is below the critical dispersion $c_r = 3.36G\mu/\kappa$ (where μ is the gas surface density, and κ the epicyclic frequency) for axisymmetric instability (Toomre criterium, 1964), the unstable structures formed heat up the gas until it reaches the minimal dispersion again. We can compute the value of the critical dispersion c_r in function of radius for M51 from its adopted rotation curve (see fig. 2). This does not contribute enough turbulent velocity to increase significantly the viscous torques efficiency. We therefore believe unlikely that large-scale gravitational instability heating can broaden line-widths up to 60km/s.

Also, the characteristic decay-time τ of the turbulence can be estimated from the dissipation rate per unit mass $=v_l{}^3/l$ (Landau & Lifchitz, 1954) and the energy per unit mass = $V_{rot}{}^2 = (200km/s)^2$ by: $\tau = l \times V_{rot}{}^2/v_l{}^3 = 10^8$ yrs, which is quite unrealistic (for $v_l = 10km/s, \tau = 2 \times 10^{10}$yrs). Indeed, that means that all the gaseous disk should have collapsed towards the center in about 10^8yrs, while the period of the orbit of the companion NGC 5195 is a few 10^9yrs, and the long HI tail observed with the VLA (Rots et al 1990) suggests that we are contemplating its second passage around M51. It could be argued that the interaction is becoming much stronger, since due to dynamical friction, the companion might be spiraling down quickly. In case of such strong dynamical perturbations, it can be shown that viscous torques are negligible with respect to gravitational torques to alter the angular momentum of the gas (Combes et al 1990).

In the present simulations, we take into account the gravitational perturbation of the companion, and the induced spiral structure; we reproduce with the correct order of magnitude the corresponding velocity perturbations (streaming motions), yet we do not obtain such a high turbulent velocity, either in the plane, or perpendicular to it. We measure $\sigma_v = 8km/s$ in the plane, in pixels 250 pc large (in the perpendicular direction, the scale-height of the potential is a free parameter, and could perturb the estimation).

An alternative explanation would be the existence of a thick disk in the center of M51: with 60km/s velocity dispersion, the thickness would be of the order of 600 pc. Recently Garcia-Burillo et al (1992) have reported the detection of an extended "halo-like" molecular component (which extends up to z $\sim$ 1 kpc), coexisting with a normal thin disk, in the edge-on spiral galaxy NGC891. If viewed face-on, high-z gas could contribute to enlarge the spectra (as σ_z scales as $\sim$ z). However the amount of molecular mass contained in the halo seems too small (20% of the total mass) and the possible widening of the spectra would be very limited. Moreover, the spectrum would consist of two gaussian components: a narrow line associated with the thin disk and a much broader gaussian superposed as a plateau to the normal emission and contributing 1/5 of the total integrated intensity. This is definitely not the shape of the observed spectra, so we can probably discard a similar scenario in M51.

What happens in other external galaxies? (see table 2)In M31, CO line-widths are of the order of 10-25km/s with 100 pc resolution (Boulanger et al 1984), and somewhat larger with 340 pc resolution, due to the systematic gradient in the beam (Boulanger et al 1981). Casoli & Combes (1988) have resolved a single GMC in M31, with a maximum antenna temperature of 0.7K, and linewidth 15km/s. This is coherent with the low excitation temperature of envelopes of giant molecular complexes. In NGC6946 (Casoli et al 1990), the line-width in the CO(1–0) line at 570 pc resolution is of the order of 20km/s in the bright arms, and even lower outside. This suggests that opacity effects are less severe than in M51: indeed, the total H_2 mass detected in NGC6946 is 10 times less than in M51 (Clausset, 1990). IC342 has also line-widths of the order of 50-60km/s (Eckart et al 1990), at 500 pc or 250 pc resolution as well (CO(1–0) and CO(2–1) lines respectively), in positions offset from the center; macroscopic optical thickness is also likely in this CO-rich galaxy.

5. Conclusions

We have presented a dynamical model of the molecular gas in M51, which allows to shed some light both on the structure of gas orbits and on the interpretation of the CO lines.

- 1). We find that the main optical and molecular spiral structure of M51 lies between the inner Lindblad resonance and the corotation. The inner oval ends up just at the ILR.

- 2). Inside the molecular "ring", the gas orbits are parallel to the oval distortion, but they rotate as soon as the ring begins. The ring is formed by depopulation of the center by the gravitational torques of the perturbation.

- 3). Our simulations reproduce satisfactorily the observed high arm-interarm contrasts merely by orbit-crowding. We do not need to invoke the formation of molecular clouds from HI complexes to reproduce the contrasts. We do not see evidence for large-scale galactic shocks, either in the observations, nor in the simulations.

- 4). We also reproduce the streaming motions in the arm and in the interarm regions with the right order of magnitude. The kinematical effect of the central bar, inducing non-circular motions (elliptical orbits) is visible both in the observations and in the simulations.

- 5). The velocity dispersion observed in the CO profiles is enhanced in the arms, both in the observations and in the model. Nevertheless, the observed line-widths are systematicaly a factor 2 higher in the in-arm observed spectra, than in the model. We propose two explanations accounting for such discrepancy: Macroscopic opacity effects, caused by a surface filling factor higher than 1, and large-scale turbulence fueled by the dissipation of the kinetic energy (provided by the differential rotation in the disk) by viscous torques. Locally, expanding shells due to supernovae could also broaden the spectra.

  By considering macrosopic opacity, we succeeded in increasing locally the line-widths. Moreover, that does not seem enough. On the other hand, the large scale turbulence could explain locally (at R $\sim$ 2 kpc) the observed velocity dispersion, although it imposes a surprisingly short life-time for the molecular disk ($\sim$ 1 rotation period).

Acknowledgements. The calculations have been done on the CRAY-2 of the "Centre de Calcul Vectoriel pour la Recherche" (CCVR), Ecole Polytechnique, Palaiseau (France). We thank Dr. Gatley for providing us with his infrared CCD image and the MAMA staff for helping us in digitizing the red plate. S.Garcia-Burillo thanks the Spanish CICYT (grant number PB88-0453) for its partial economic support.

References

Bloemen, J.B.G.M. et al., 1986: *Astron. Astrophys.* **154**, 25

Boulanger F., Stark A.A., Combes F.: 1981 *Astron.Astrophys.* **93**, L1

Boulanger F., Bystedt J., Casoli F., Combes F.: 1984 *Astron.Astrophys.* **140**, L5

Brouillet, N., Baudry, A., Combes, F.:1988 *Astron. Astrophys.* **196**, L17

Casoli, F., Clausset, F., Viallefond, F., Combes, F., Boulanger, F. 1990 *Astron. Astrophys.*, **233**, 357

Casoli, F., Combes, F., 1988 *Astron. Astrophys.*, **198**, 43

Clausset F. (1990), PhD thesis, Université Paris 6.

Combes F., Gerin M.: 1985, *Astron.Astrophys.* **150**, 327

Combes F., Dupraz C., Gerin M.: 1990, in *Dynamics and Interactions of Galaxies*, ed. R. Wielen, Springer-Verlag Heidelberg, page 205

Combes F.: 1991, in *Dynamics of Galaxies and their Molecular Cloud Distributions*, ed. F. Combes & F. Casoli, Kluwer, IAU 146, page 255

Combes F.: 1991, *Ann.Rev.Astr.Astrophys.* **29**, 195

Contopoulos G., Papayanopoulos T.: 1980, *Astron.Astrophys.* **92**, 33

Dickey J.M., Hanson M.M., Helou G.: 1990, *Astrophys.J* **352**, 522

Eckart, A., Downes, D., Genzel, R., Harris, A.I., Jaffe, D.T., Wild, W., 1990 *Astrophys.J* **348**, 434

Elmegreen B.G.: 1991, in *Fragmentation of Molecular Clouds and Star Formation*, ed. E. Falgarone, F.Boulanger & G. Duvert, Kluwer, IAU 147, page 205

Falgarone E., Phillips T.G.: 1990, *Astrophys.J* **359**, 344

Fleck R.C.: 1981, *Astrophys.J.* **246**, L151

Garcia-Burillo S., Guélin M.: 1990, in *Dynamics of Galaxies and their Molecular Cloud Distributions*, ed. F. Combes & F. Casoli, Kluwer, IAU 146, page 67

Garcia-Burillo S., Guélin M., Cernicharo, J., Dahlem, M., 1992 *Astron. Astrophys., in press*

Garcia-Burillo S., Guélin M., Cernicharo, J., Paper I, 1992 *submitted to Astron. Astrophys.*

Hernquist L. 1990, in *Dynamics and Interactions of Galaxies*, ed. R. Wielen, Proceedings of Heidelberg, Springer-Verlag, page 108

Howard S., Byrd G.G.: 1990, *Astron.J* **99**, 1798

Landau L.D., Lifshitz E.M. (1954) Hydrodynamica (Ed. Mir, Moscow)

Lin D.N.C., Pringle J.E.: 1987 *Month.Not.Roy.Ast.Soc* **225**, 607

Lo K.Y., Ball R., Masson C.R., Phillips T.G., Scott S., Woody D.P.: 1987, *Astrophys.J.* **317**, L63

Lo K.Y., Adler D.S., Allen R.J., Plante R., Wright M.C.H., Rydbeck G.: 1991 in *Dynamics of Galaxies and their Molecular Cloud Distributions*, ed. F. Combes & F. Casoli, Kluwer, IAU 146, page 81

Lynden-Bell D., Pringle J.E.: 1974 *Month.Not.Roy.Ast.Soc* **168**, 603

McKee C.F., Ostriker J.P.: 1977,*Astrophys.J* **218**, 148

Myers P.C., Goodman A.A.: 1988, *Astrophys.J* **326**, L27

Pierce M.J.: 1986,*Astron.J* **92**, 285

Planesas, P., Gómez-González, J., Martin-Pintado, J., 1989 *Astron. Astrophys.* **216**, 1

Polk K.S., Knapp G.R., Stark A.A., Wilson R.W.: 1988,*Astrophys.J* **332** , 432

Rand R.J., Kulkarni S.R.: 1990, *Astrophys. J* **349**, L43

Rots A.H., Bosma A., van der Hulst J.M., Athanassoula E., Crane P.C.: 1990, *Astron.J* **100**, 387

Rickard, L.J., Turner, B.E., 1977: *Astrophys. J* **218**, L51

Rydbeck G., Hjalmarson A., Rydbeck O.E.H.: 1985, *Astron.Astrophys.* **144**, 282

Scoville N.Z., Young J.S.: 1983,*Astrophys.J* **265**, 148

Shostak G.S., van der Kruit P.C.: 1984, *Astron.Astrophys.* **132**, 20

Solomon P.M., Rivolo A.R., Barrett J.W., Yahil A.: 1987, *Astrophys.J* **319**, 730

Talbot R.J., Arnett W.D.: 1975, *Astrophys.J* **197**, 551

Tilanus R.P.J., Allen R.J.: 1988, *Astron.Astrophys.* **330**, 667

Toomre A.: 1964, *Astrophys.J* **139**, 1217

Toomre A. 1981, in *The Structure and Evolution of Normal Galaxies* eds S.M. Fall & D. Lynden-Bell (Cambridge University Press, Cambridge 1981) page 111

Toomre A., Toomre J.: 1972, *Astrophys J.* **178**, 623

Tully R.B.: 1974, *Astrophys.J.Supp.Ser.* **27**, 437

van der Kruit P.C., Shostak G.S.: 1982, *Astron.Astrophys.* **105**, 351

Vogel S.N., Kulkarni S.R., Scoville N.Z.: 1988, *Nature* **334**, 402

Vogel S.N., Rand R.J., Gruendl R., Teuben P.: 1992, *Astrophys. J* preprint

Wilson, C.D., Scoville, N.: 1989 *Astrophys. J* **347**, 743

Zaritsky D., Lo K.Y.: 1986,*Astrophys.J.* **303**, 66

This article was processed by the author using Springer-Verlag LaTeX A&A style file 1990.

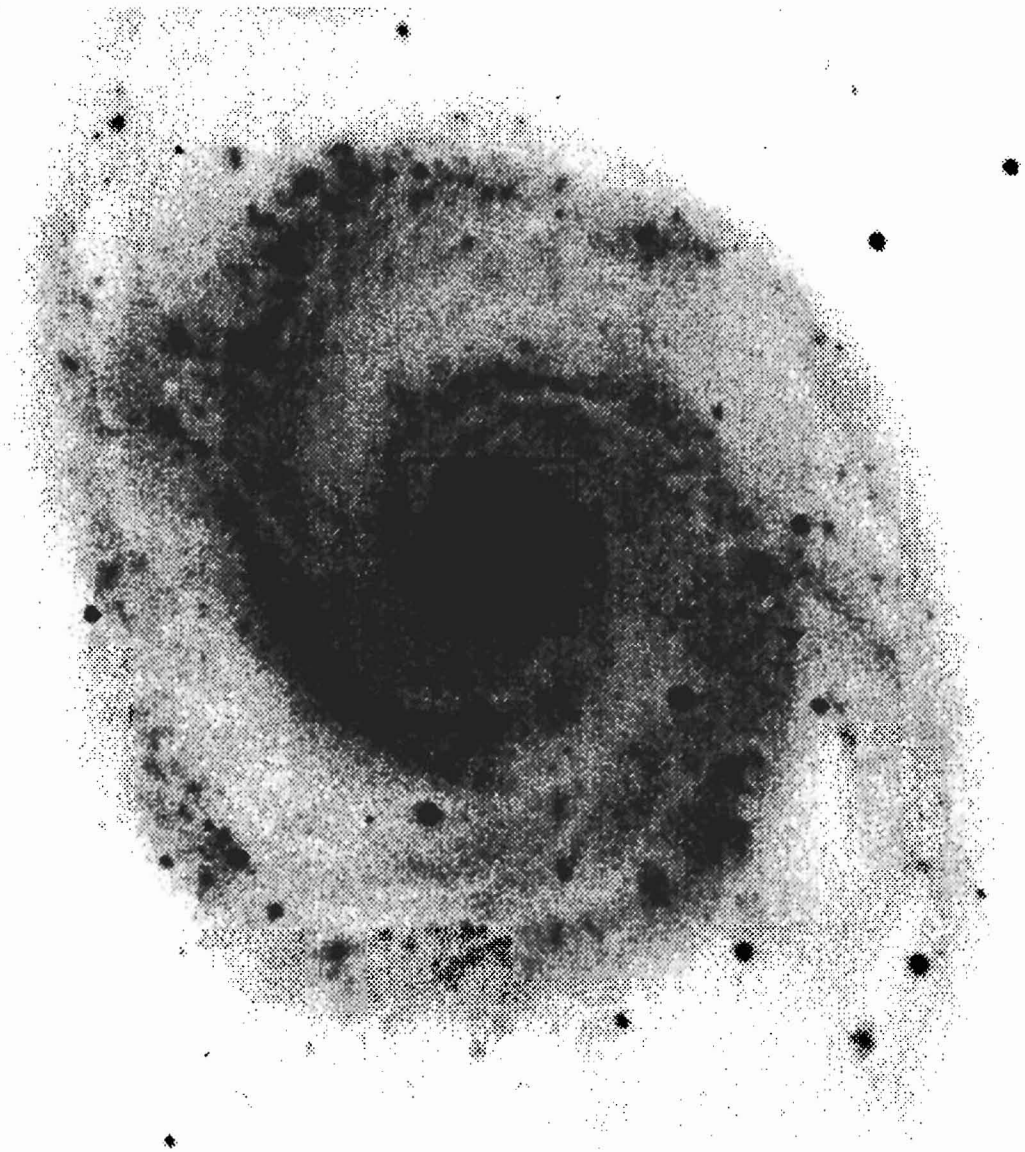

FIG 1 (Left)

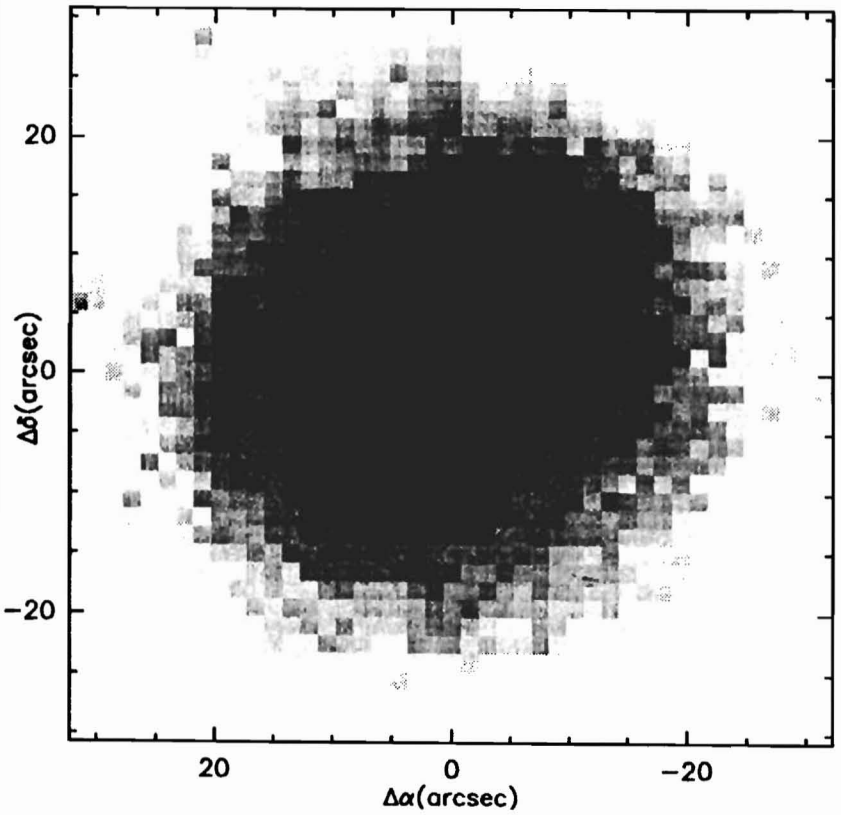

FIG1 (Right)

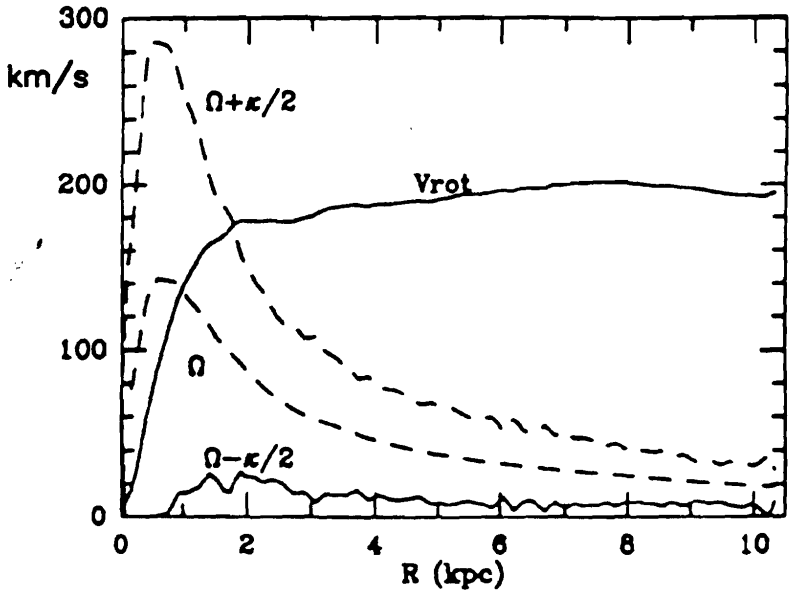

FIG. 2

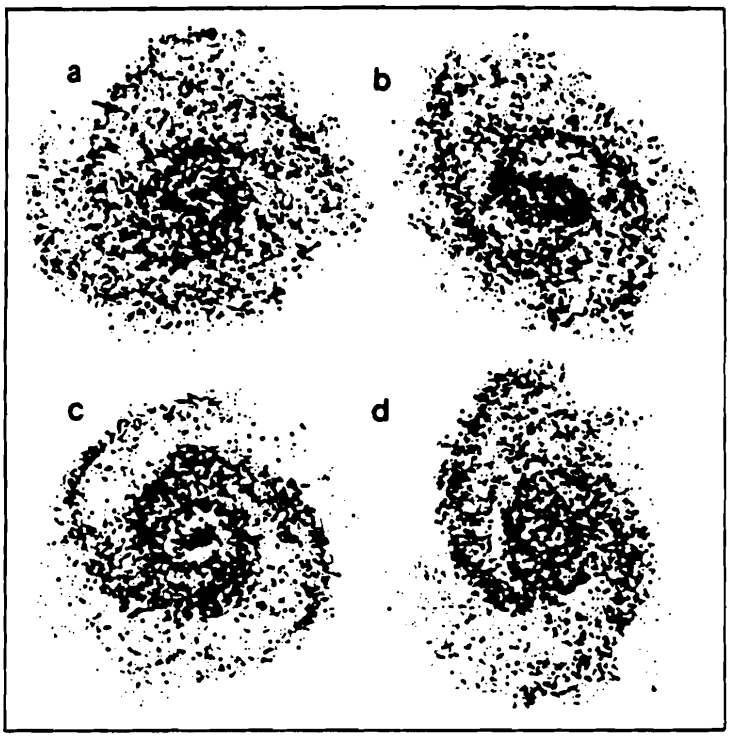

FIG.3

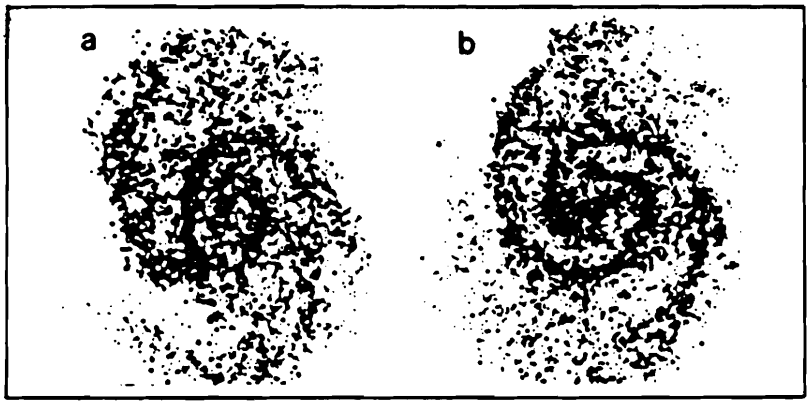

FIG. 4

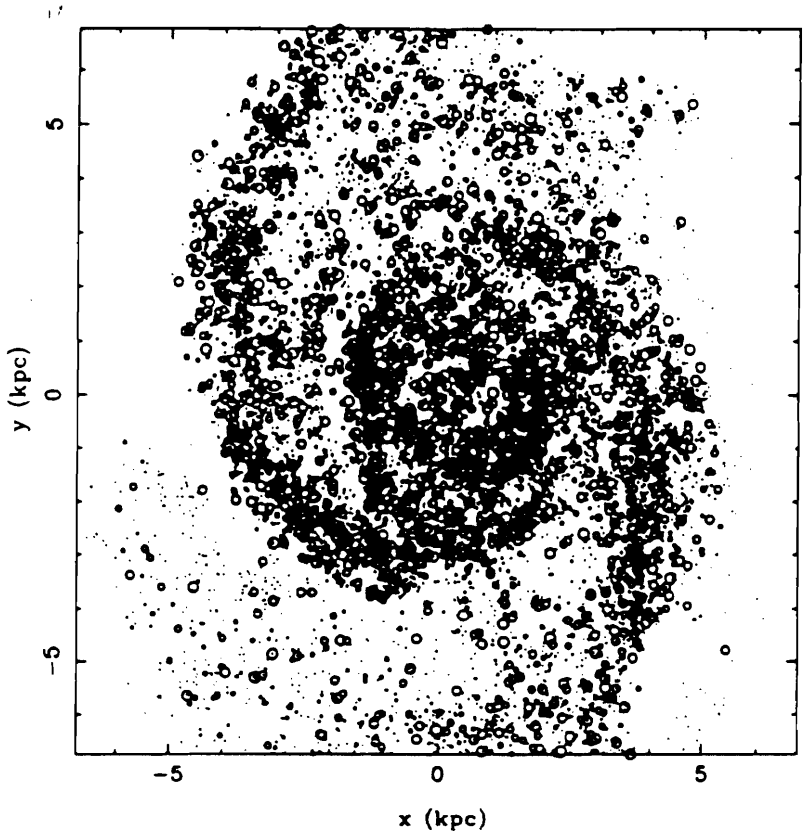

FIG. 5

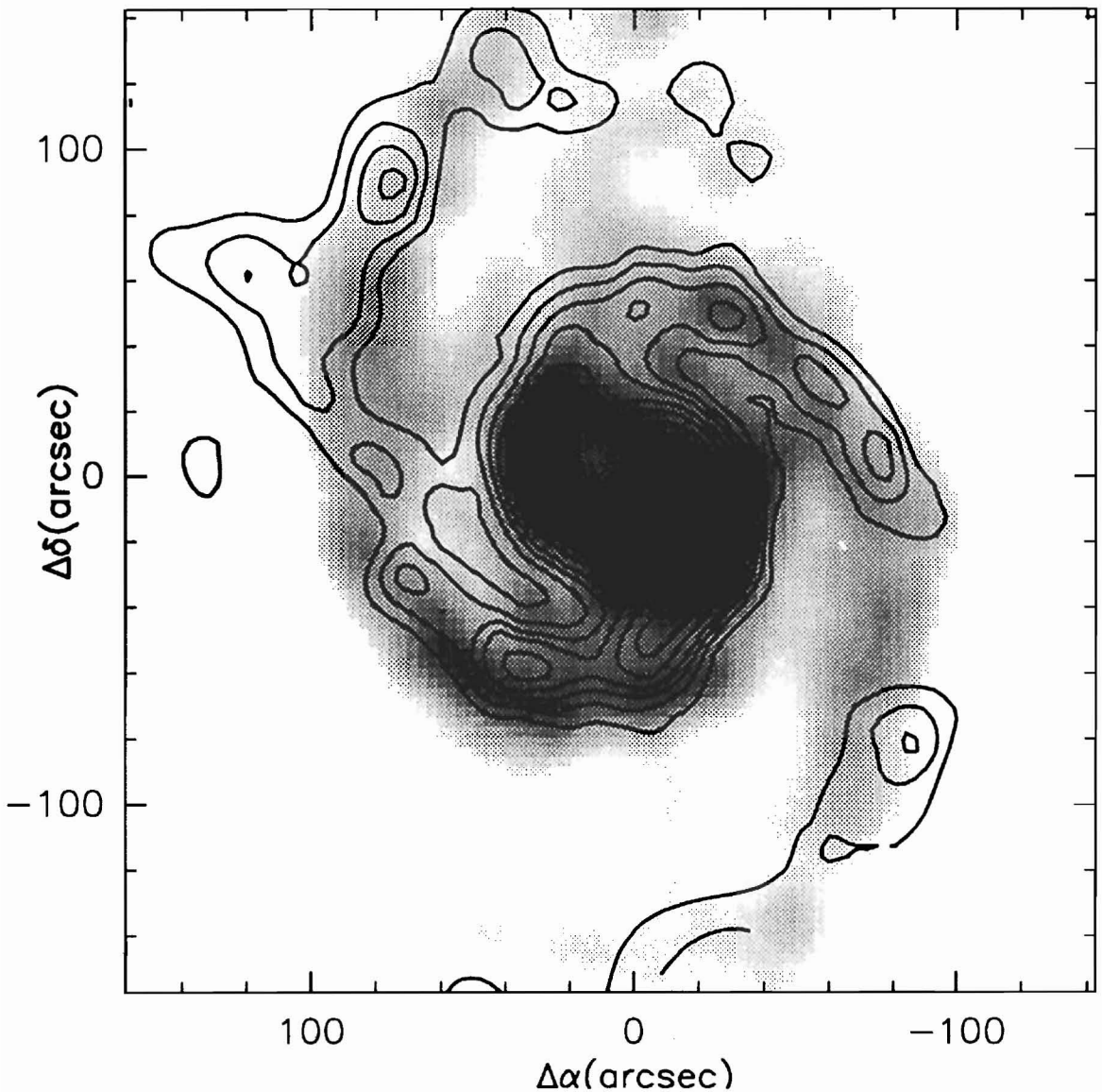

Fig 6

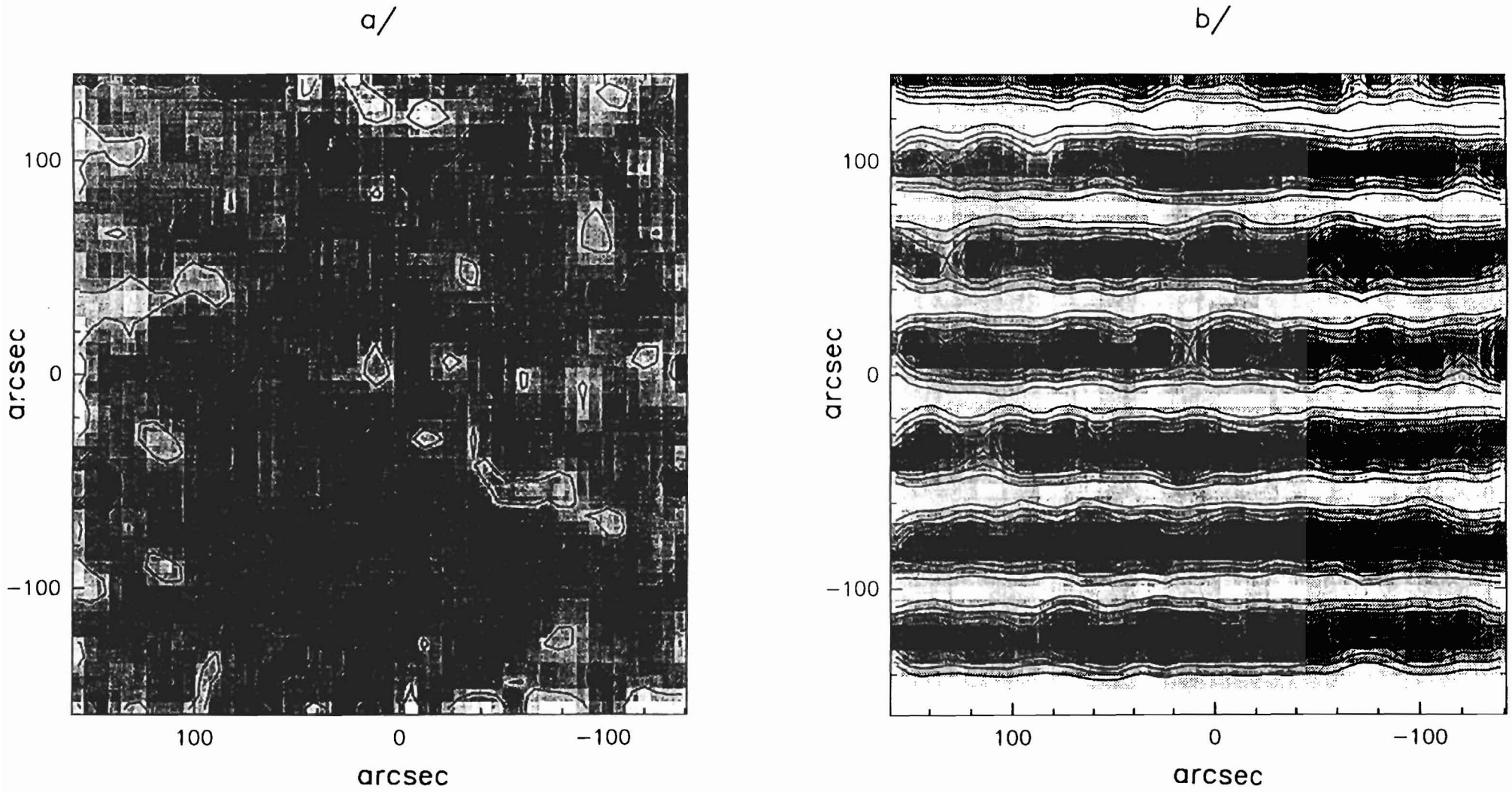
a/
b/
100
0
−100
arcsec
100
0
−100
arcsec
100
0
−100
arcsec
100
0
−100
arcsec

FIG. 7

Fig 8 a/

a/observations

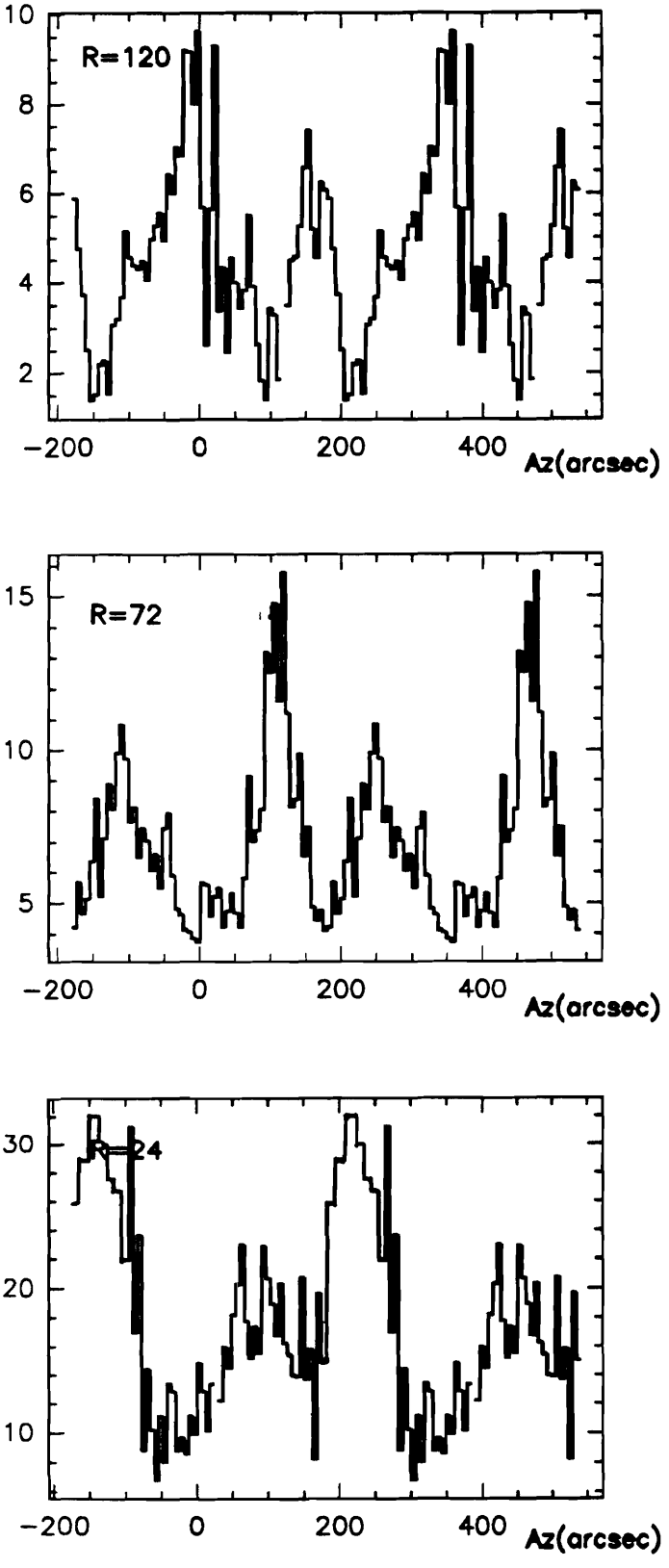

Fig 8 b/

b/opt. thin model

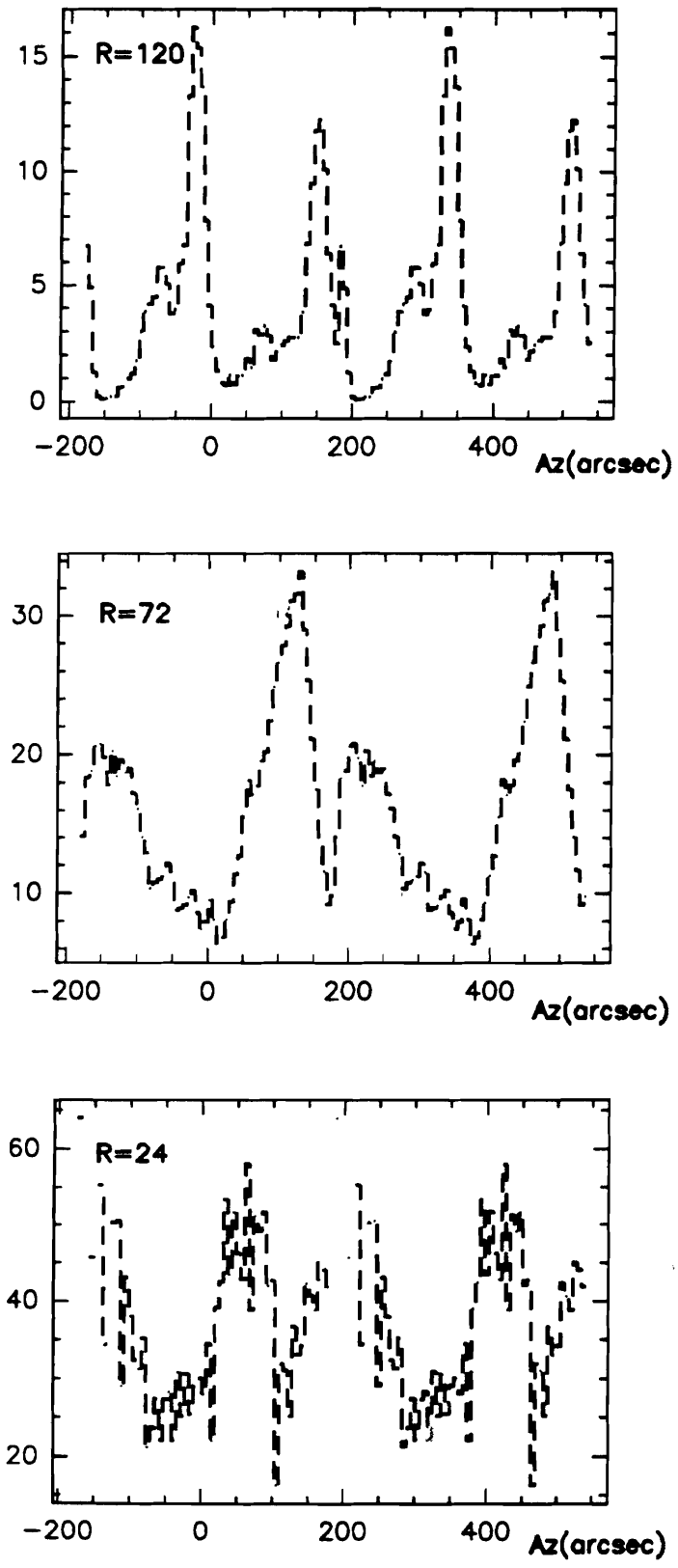

Fig. 8c

c/opt. thick model

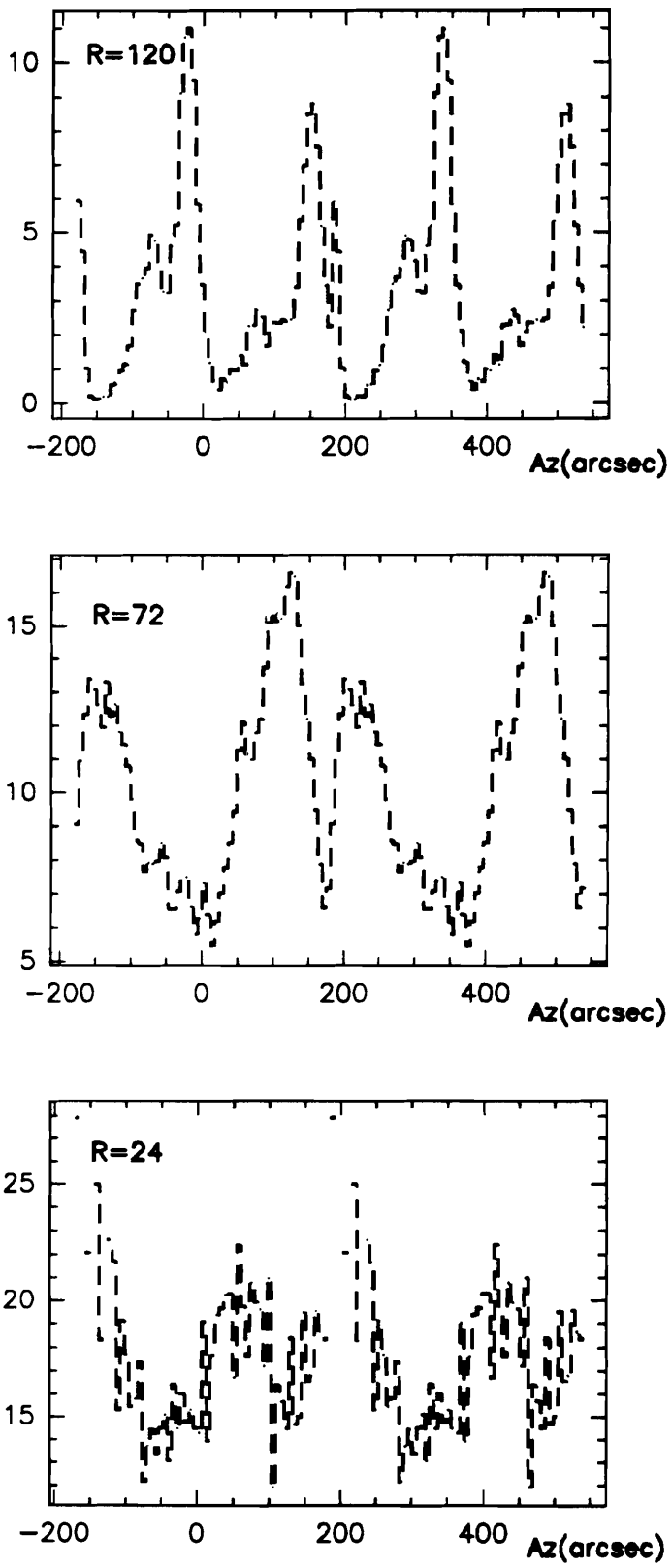

Fig. 8 d

d/infrared

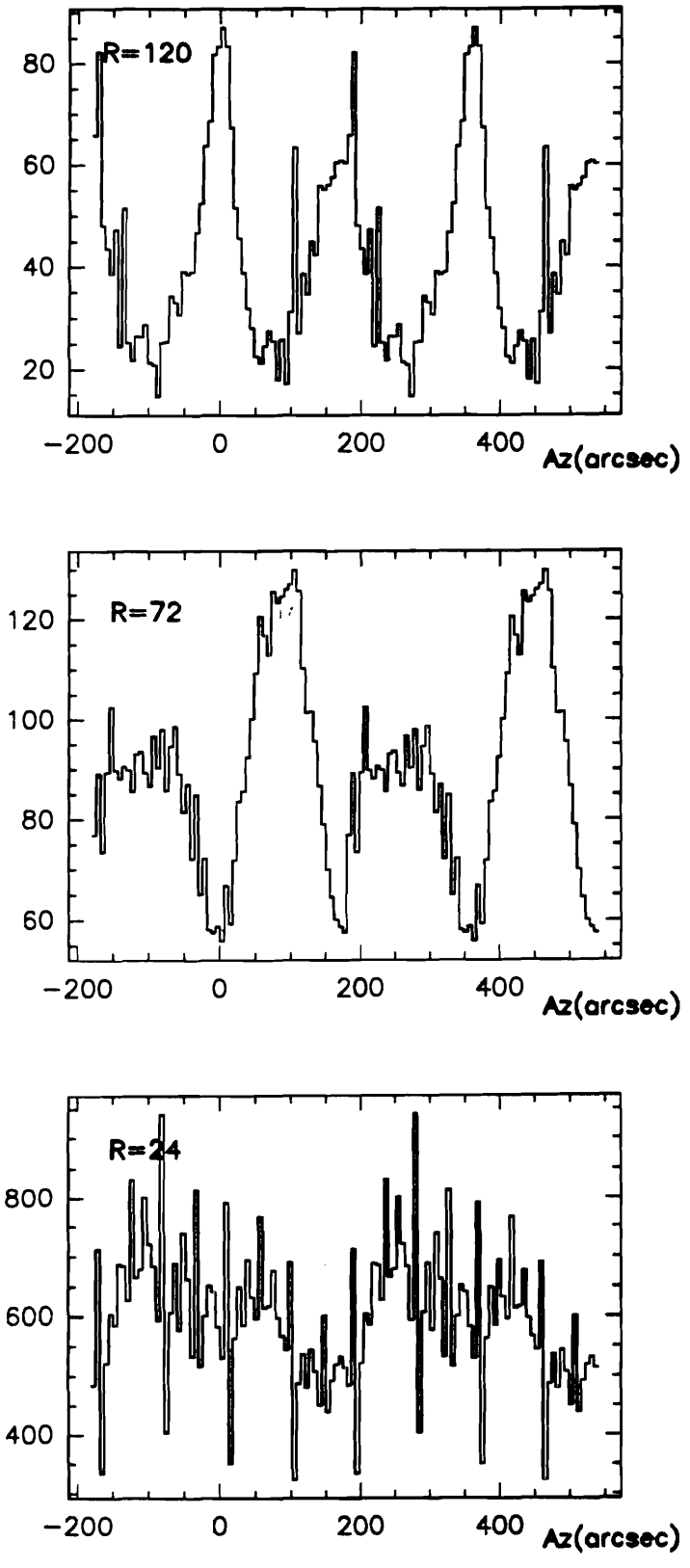

Fig. 9

obs.

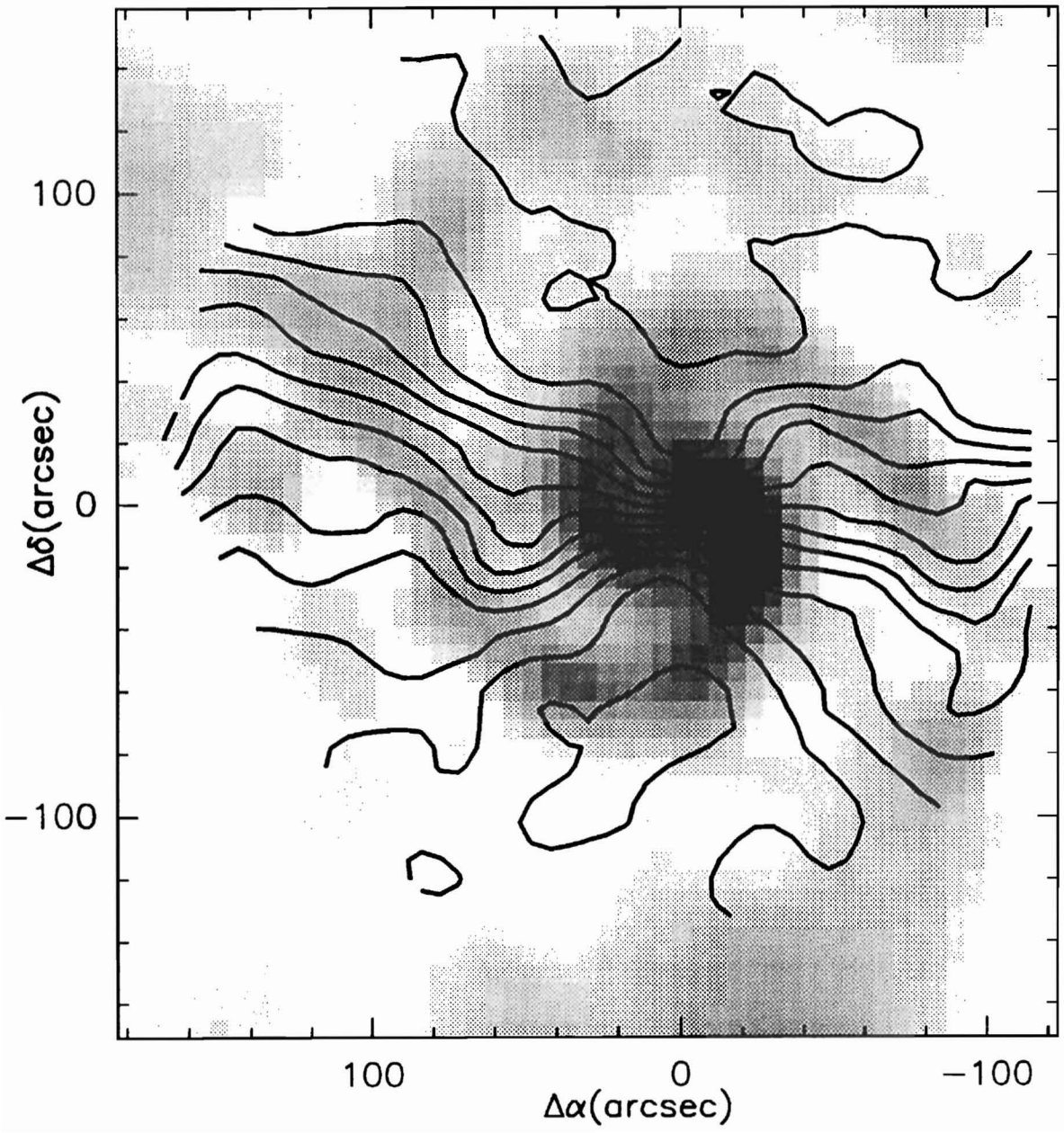

Fig 10

model

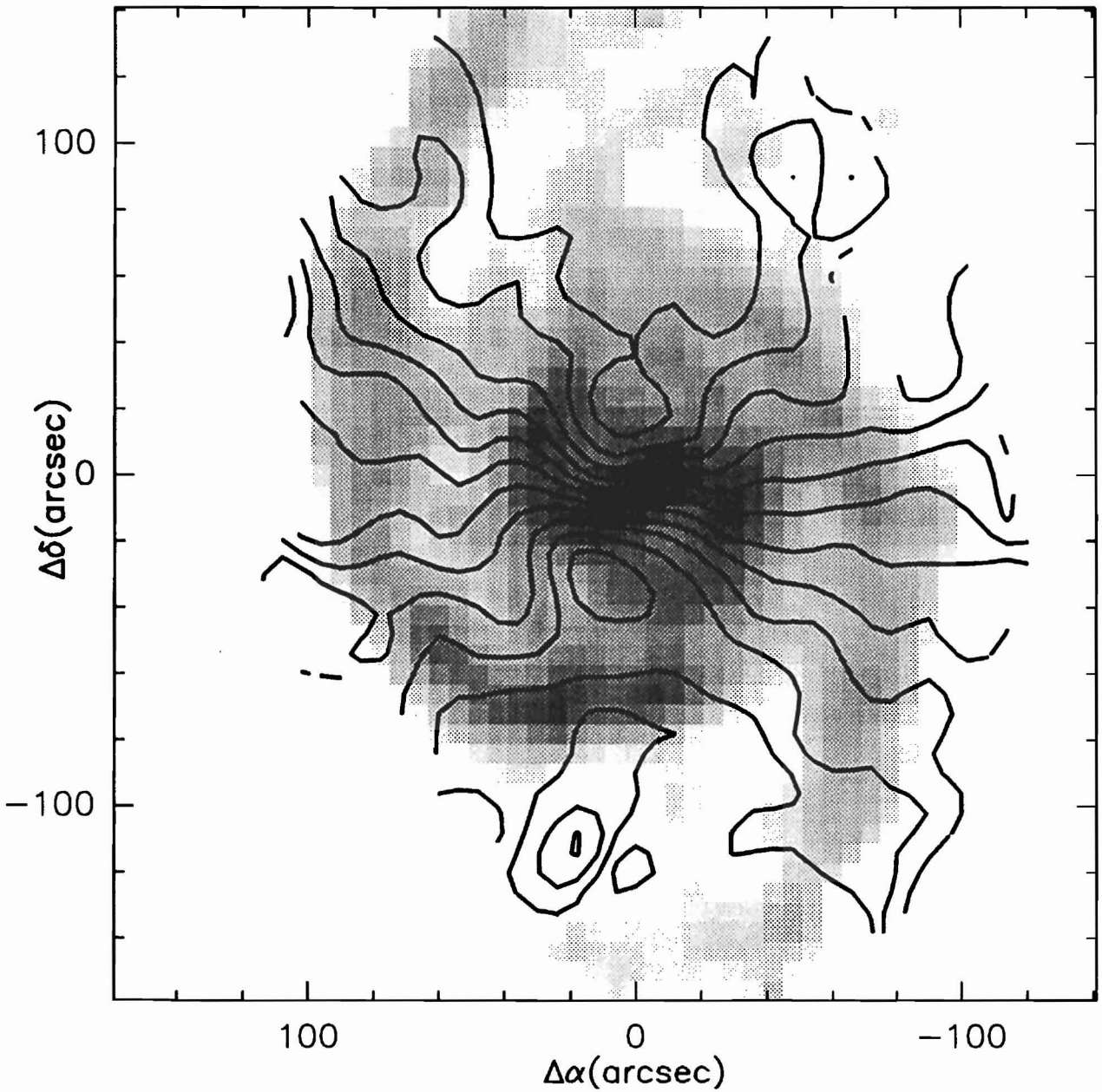

Fig 11 (top)
(observ.)

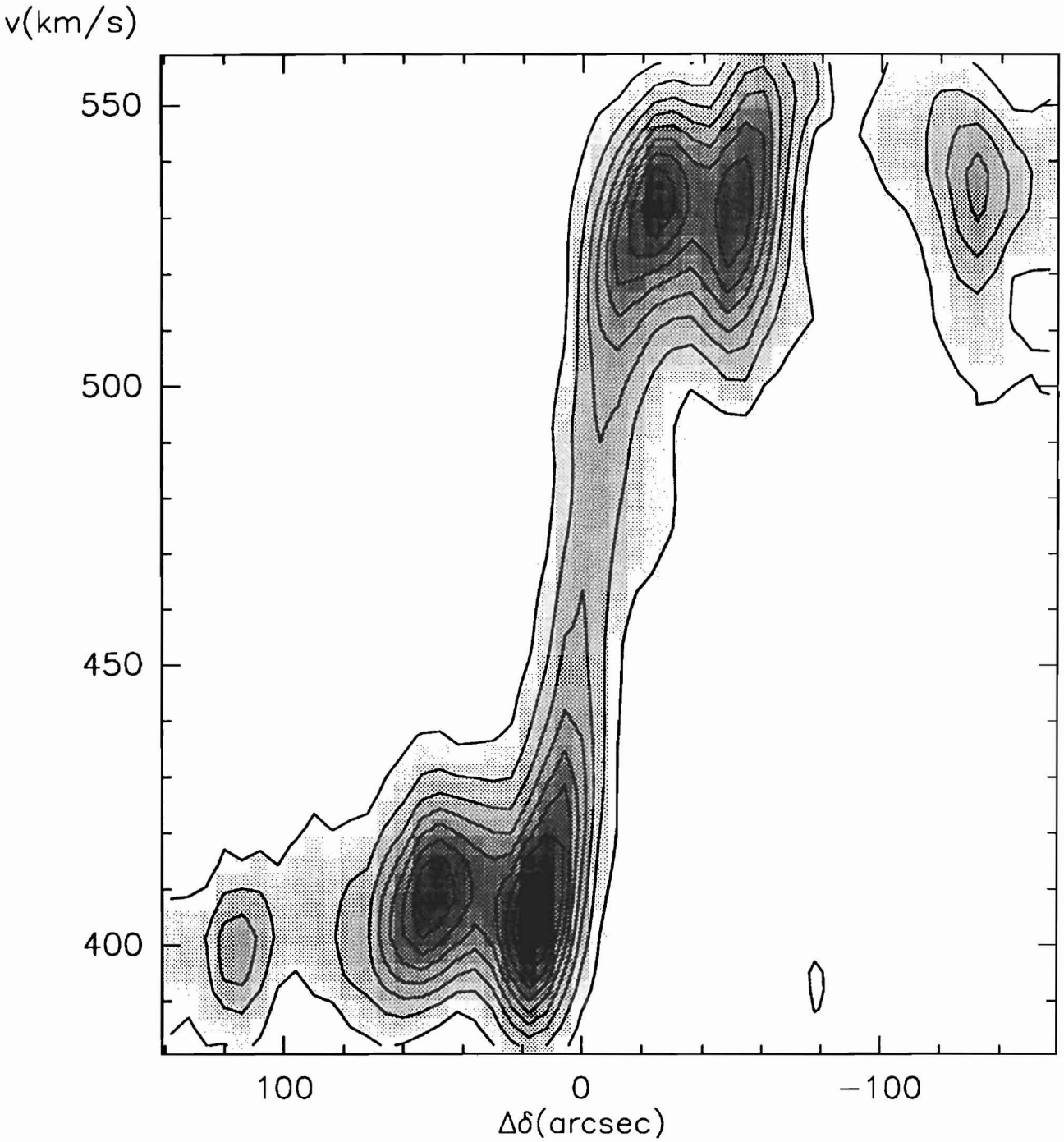

Fig 11 (bot
(model)

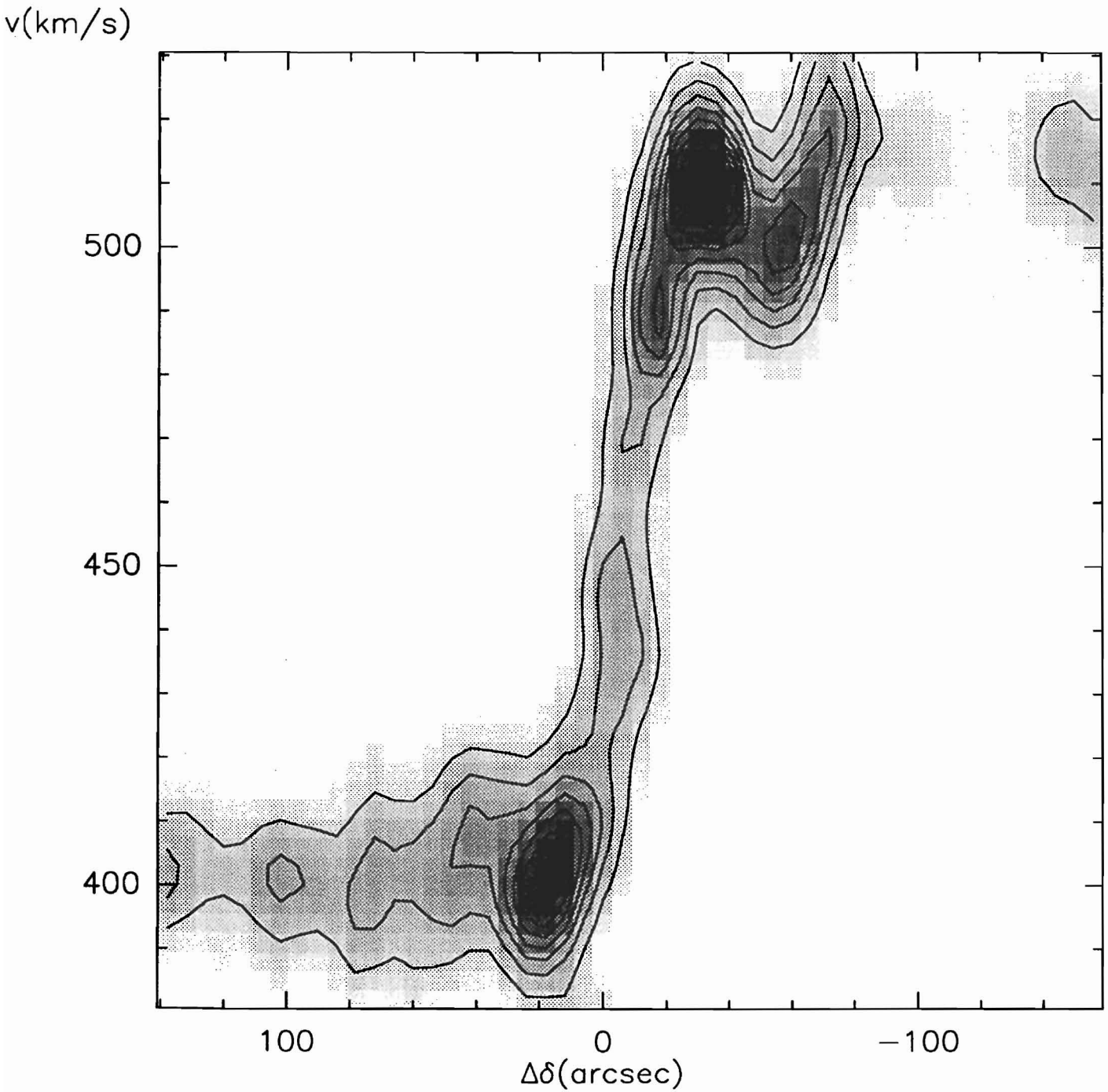

Fig 12 (observ.)

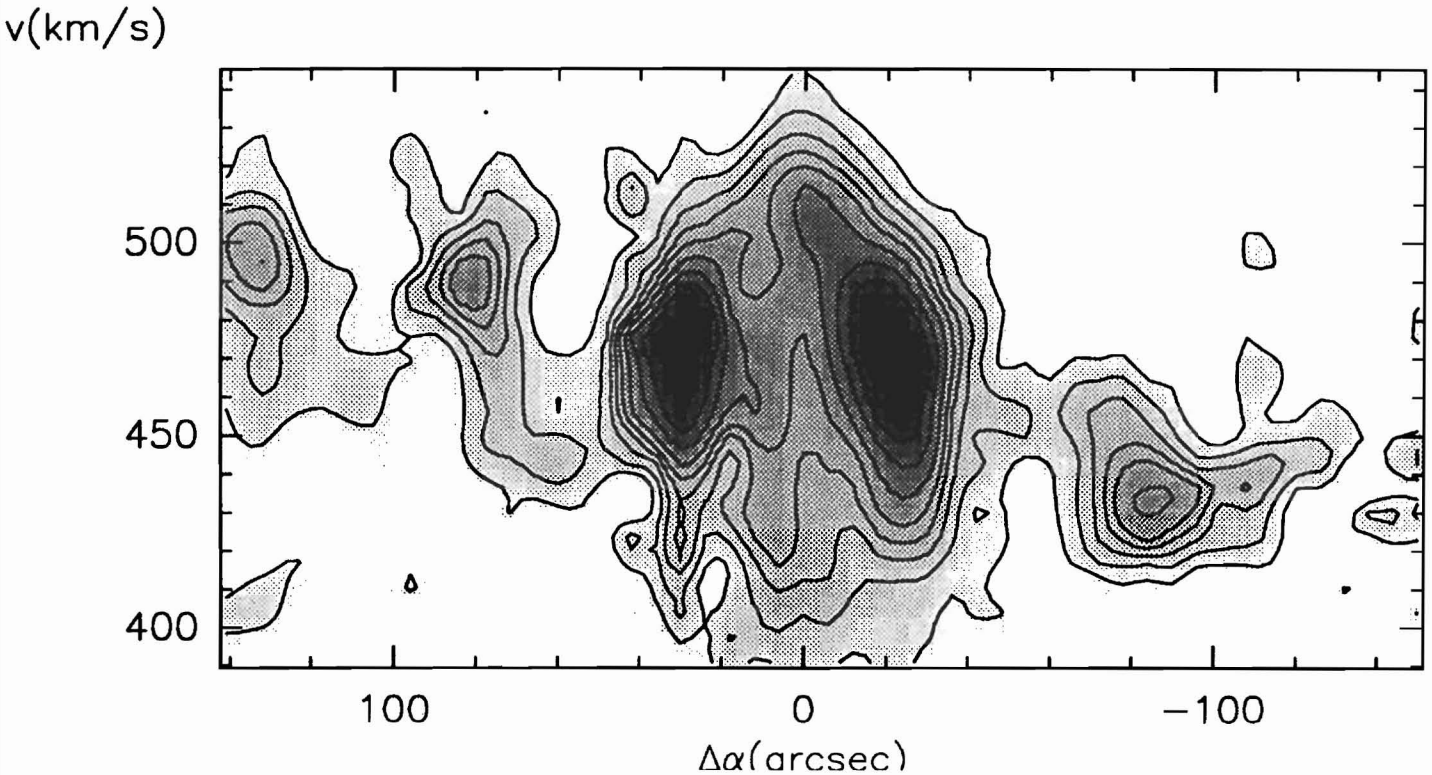

Fig. 12 / Jet
(model)

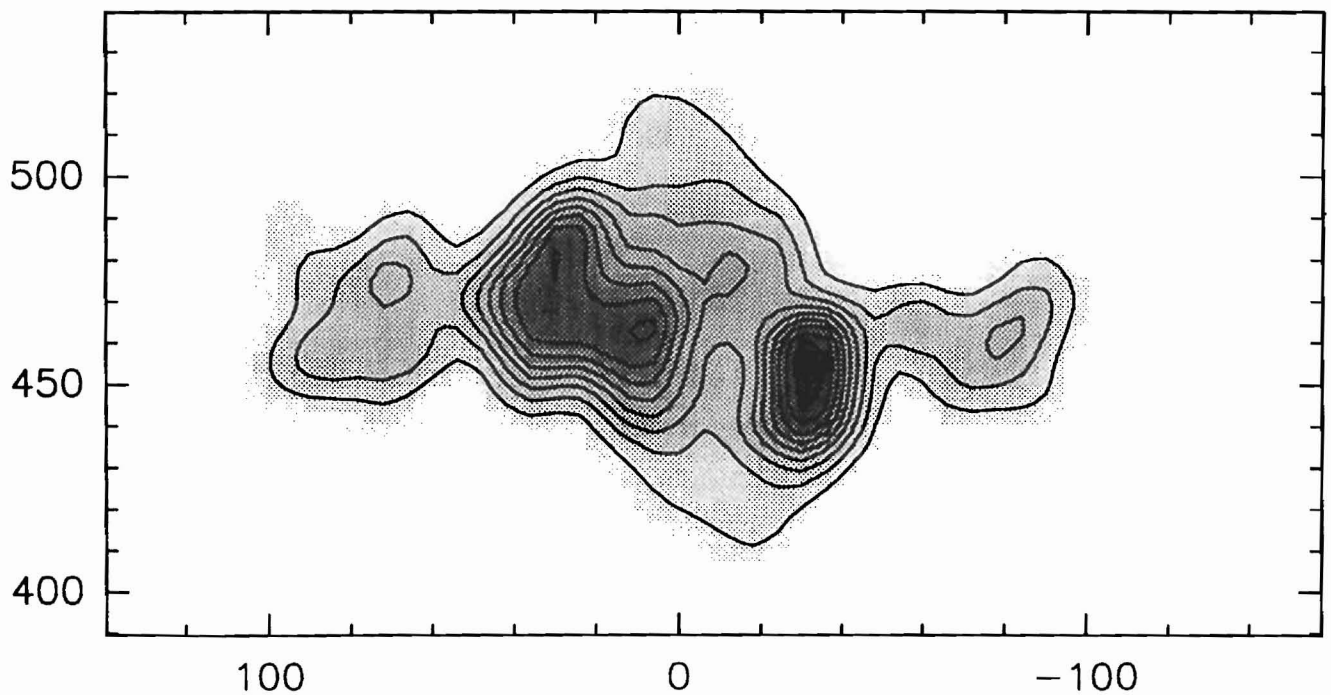

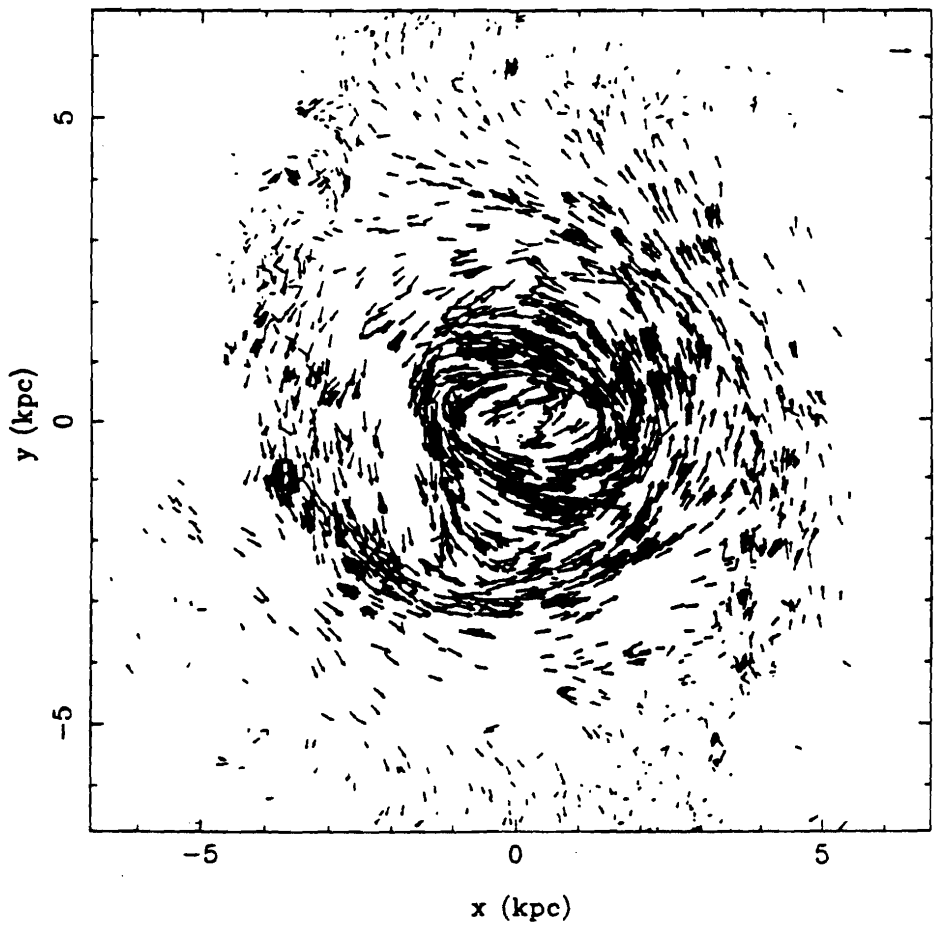

FIG. 13

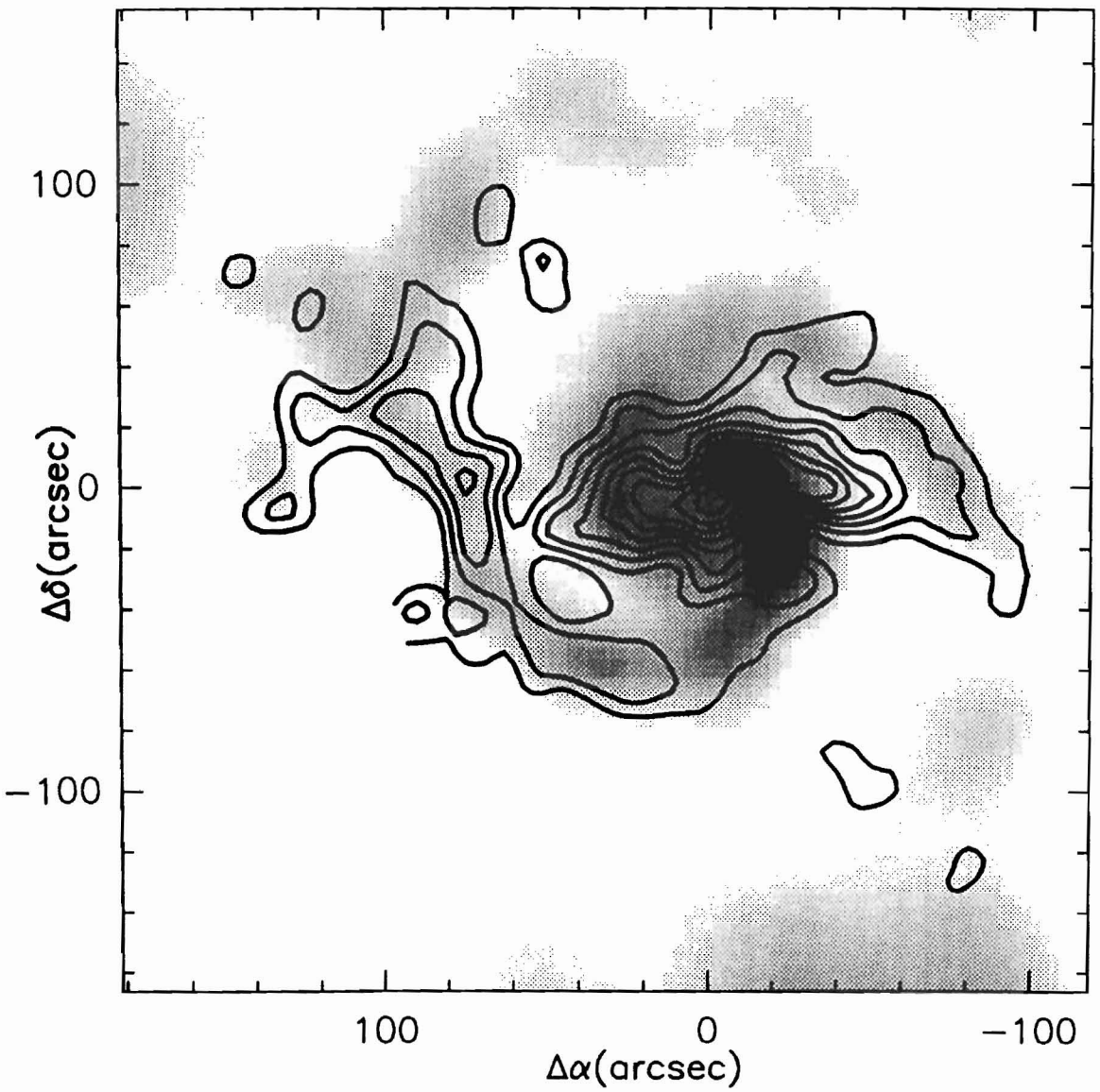

Fig 14. A/
(observ.)

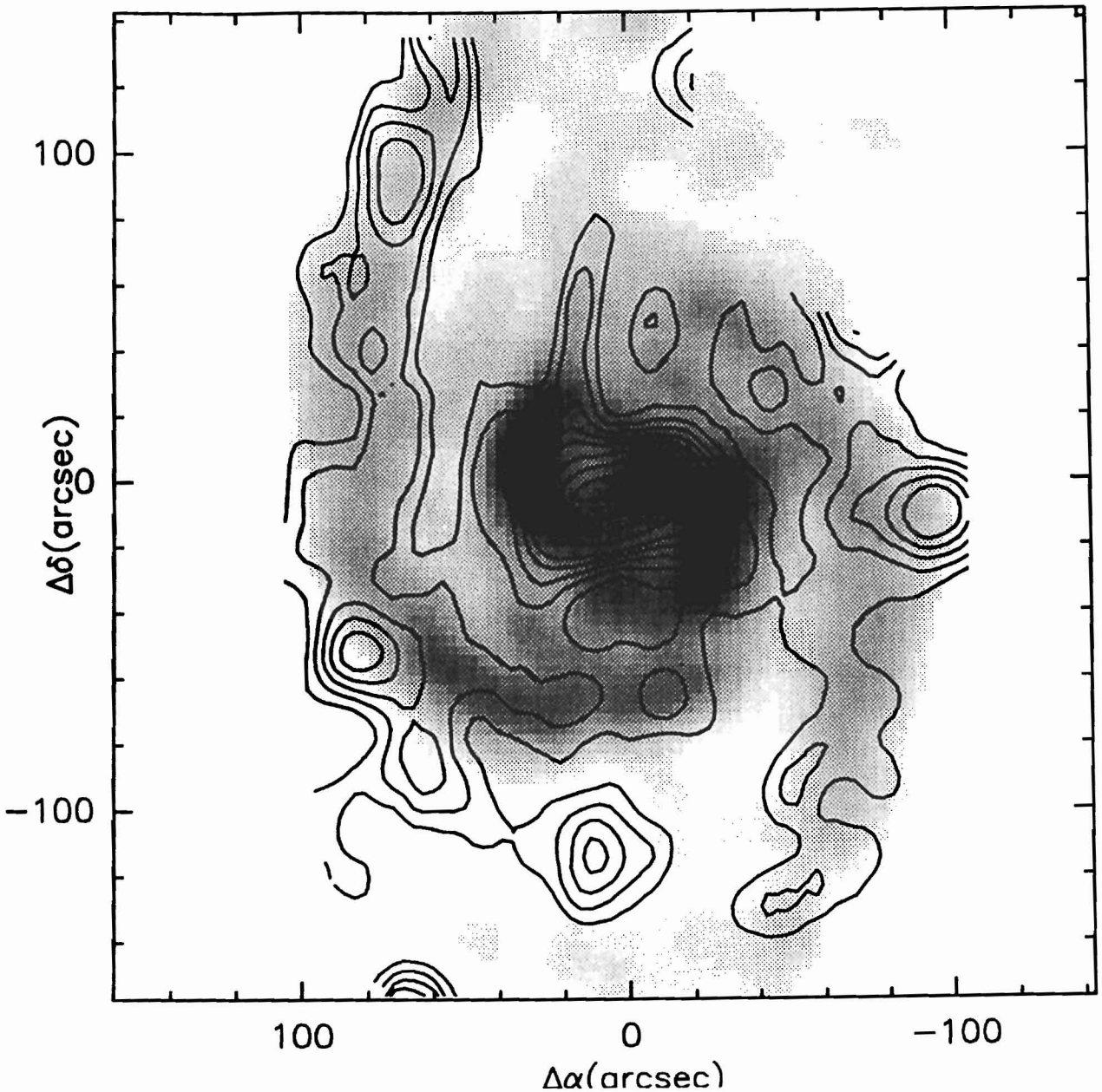

Fig 14 B/
(model)

Fig. 15

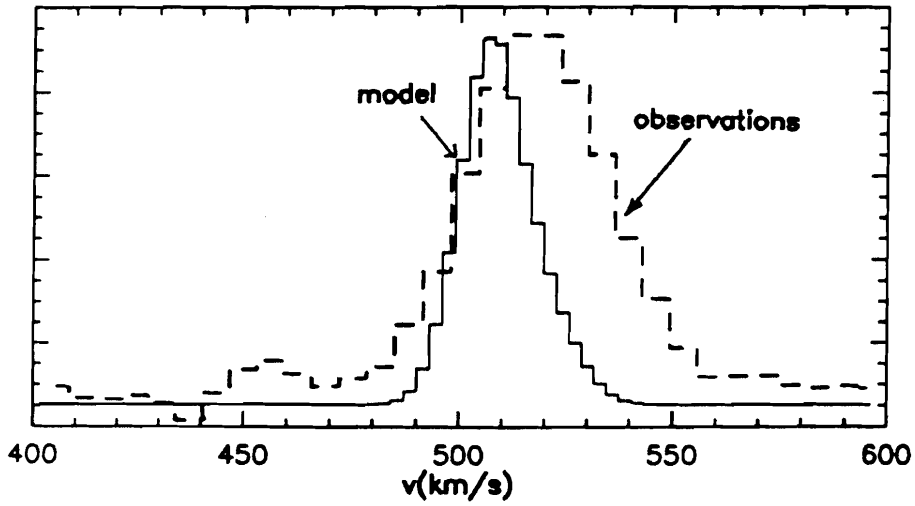

Fig. 16 a/

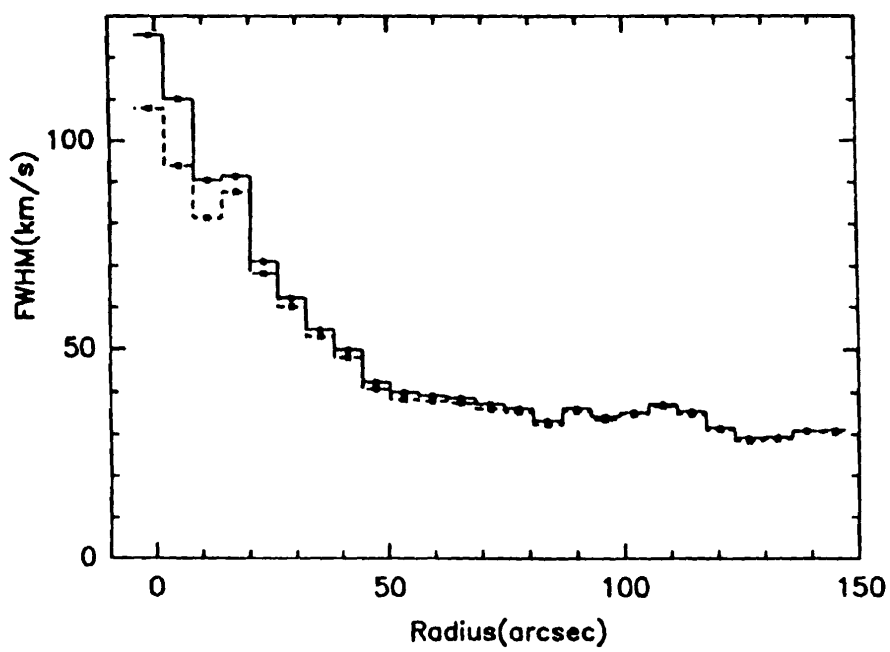

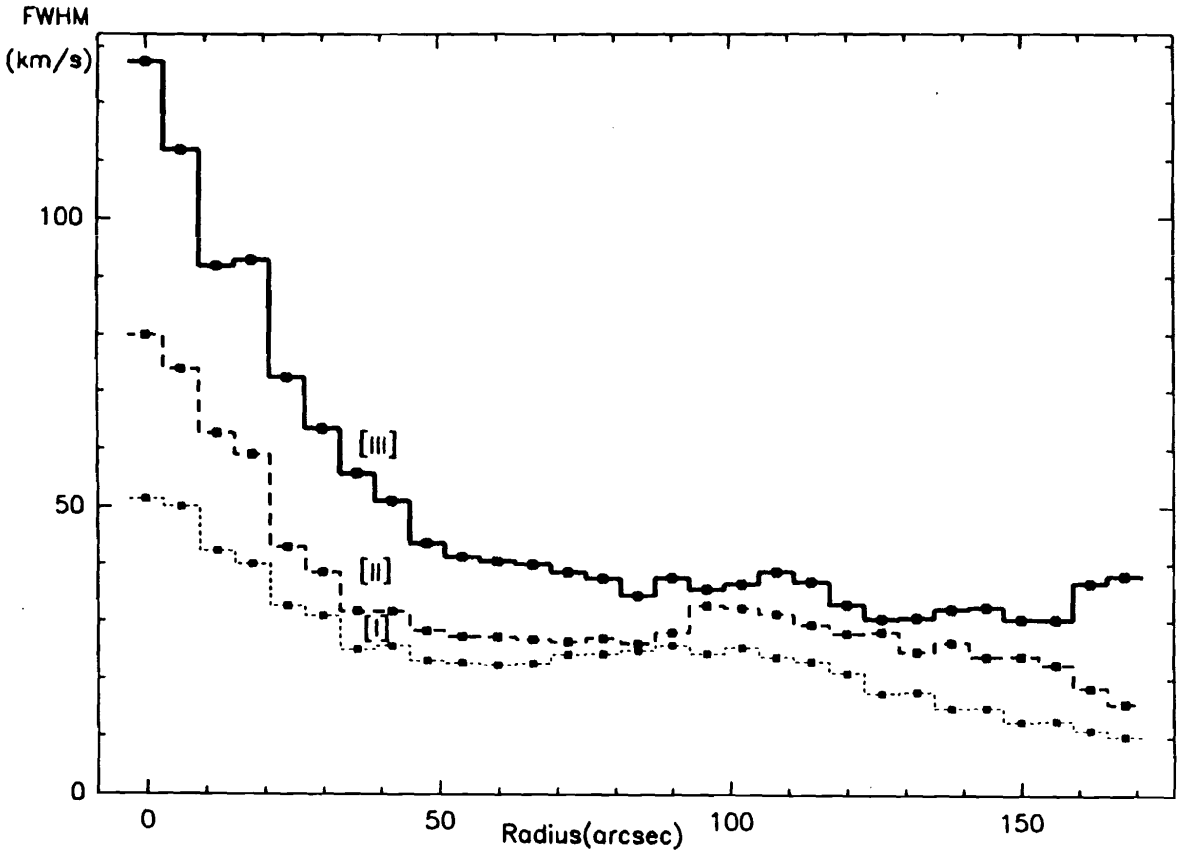

Fig 16 b/

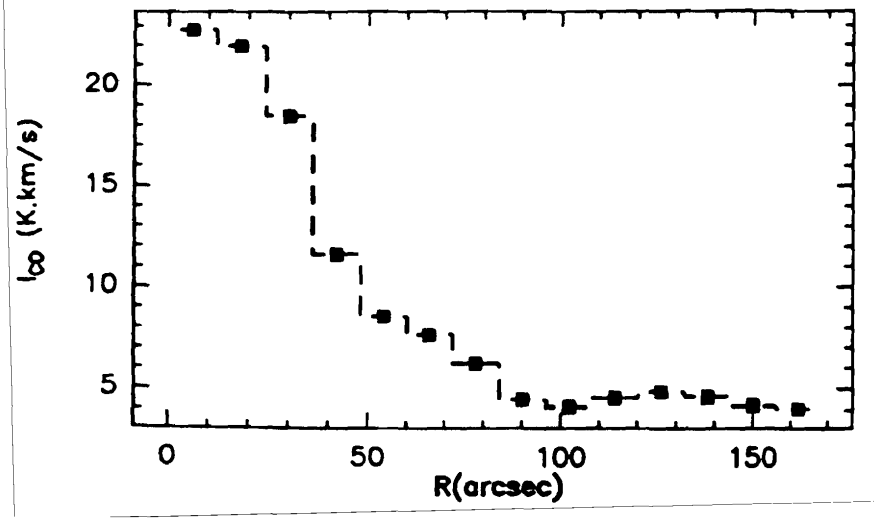

Fig 17 (Right)

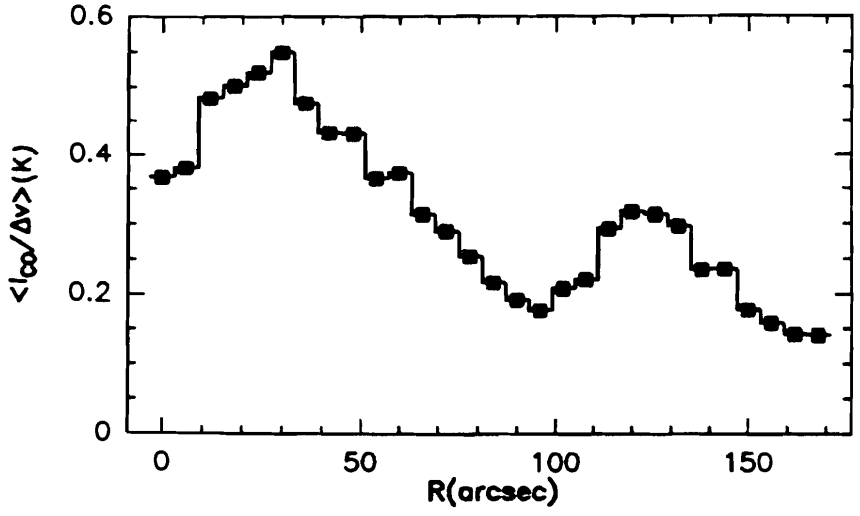

Fig. 17 (Left)

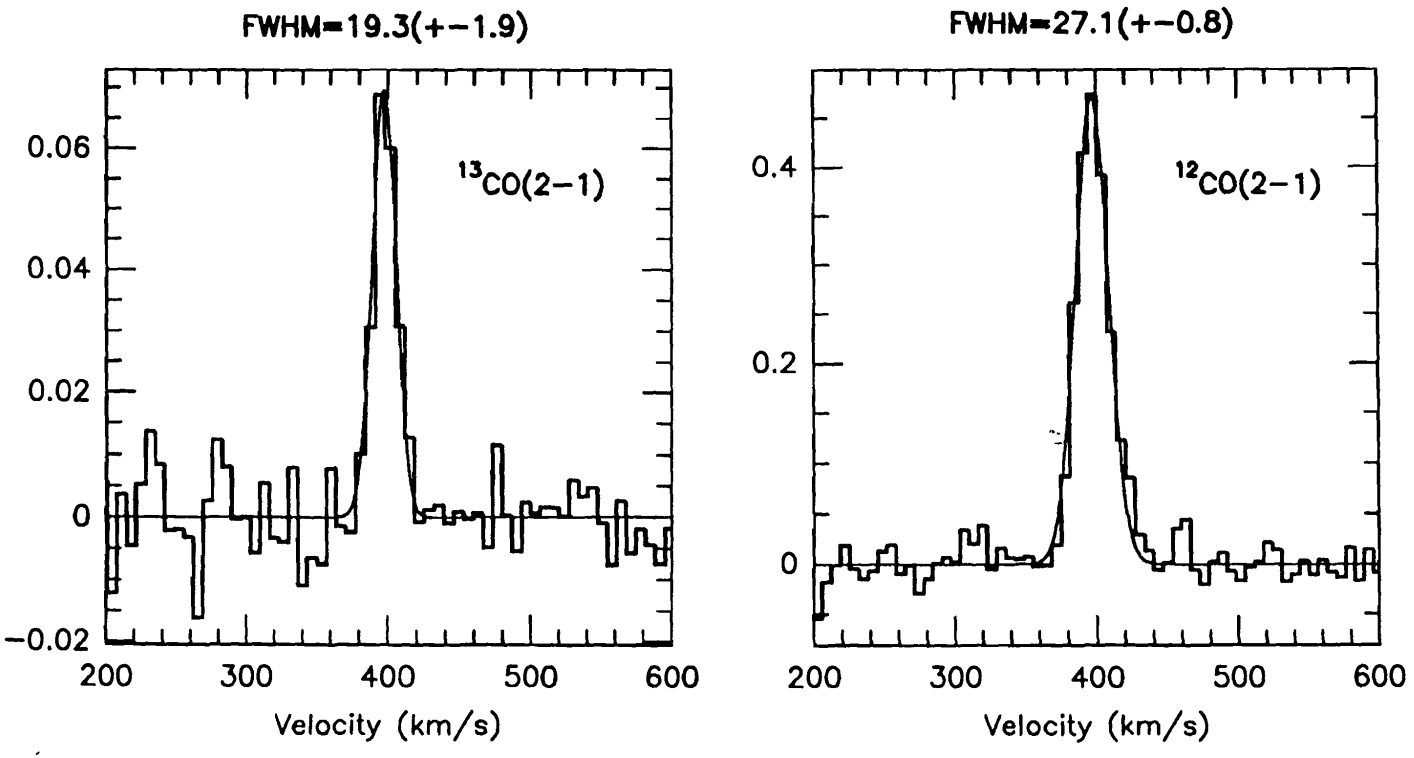
FWHM=19.3(+-1.9)
^{13}CO(2-1)
0.06
0.04
0.02
0
-0.02
200
300
400
500
600
Velocity (km/s)
FWHM=27.1(+-0.8)
^{12}CO(2-1)
0.4
0.2
0
200
300
400
500
600
Velocity (km/s)

Fig. 18

offsets (")		FWHM (kms^{-1})			
$\Delta\alpha$	$\Delta\delta$	^{13}CO(2-1)		^{12}CO(2-1)	
-24	-24	36.7	(2.4)	43.4	(0.5)
-18	-24	45.2	(2.9)	51.1	(1.2)
0	54	19.3	(1.9)	27.1	(0.8)
0	18	19.6	(3.6)	28.1	(1.4)
-30	48	37.9	(3.7)	43.4	(3.6)
-30	72	11.7	(6.9)	29.8	(5.1)
-6	0	97.2	(6.7)	110.0	(4.0)

Table 1

Table 2. CO Line-Widths (FWHM) in disks

Name	Type	D (Mpc.)	Θ(")	Size(pc)	$\Delta V(kms^{-1})$	$N(H_2)(M_\odot pc^{-2})$	References
Milky Way	Sb	0.01	45"	2.2	10	20	Solomon et al., 1987
NGC 628	Sc	9	12"	520	15	25	Braine et al., 1992 (in prep)
Maffei 2	Sbc	5	23"	560	100	100	Weliachew et al., 1988
M31	Sb	0.7	23"	77	18	11	Casoli and Combes, 1988
M81	Sb	3.2	23"	360	17	3	Brouillet et al., 1991
NGC 1068	Sb	18	12"	1050	50-60	150	Planesas et al., 1989
M33	Sc	0.8	23"	88	10	20	Viallefond et al., 1991
M51	Sc	9.5	12"	550	20-60	200	Garcia-Burillo et al., 1992
M101	Sc	7	12"	410	20	8	Viallefond et al., 1992(in prep)
IC 342	Sc	3.9	23"	430	50-60	400	Eckart et al., 1990
NGC 6946	Sc	5.5	12"	320	20	25	Casoli et al., 1990
M83	SBc	3.7	17"	300	30	35	Handa et al., 1991

Table 2